Future change of daily precipitation indices in Japan: A stochastic weather generator-based bootstrap approach to provide probabilistic climate information

Toshichika Iizumi,[1] Izuru Takayabu,[2] Koji Dairaku,[3] Hiroyuki Kusaka,[4,5] Motoki Nishimori,[1] Gen Sakurai,[1] Noriko N. Ishizaki,[6] Sachiho A. Adachi,[6] and Mikhail A. Semenov[7]

Received 28 November 2011; revised 23 April 2012; accepted 26 April 2012; published 9 June 2012.

[1] This study proposes the stochastic weather generator (WG)-based bootstrap approach to provide the probabilistic climate change information on mean precipitation as well as extremes, which applies a WG (i.e., LARS-WG) to daily precipitation under the present-day and future climate conditions derived from dynamical and statistical downscaling models. Additionally, the study intercompares the precipitation change scenarios derived from the multimodel ensemble for Japan focusing on five precipitation indices (mean precipitation, MEA; number of wet days, FRE; mean precipitation amount per wet day, INT; maximum number of consecutive dry days, CDD; and 90th percentile value of daily precipitation amount in wet days, Q90). Three regional climate models (RCMs: NHRCM, NRAMS and TWRF) are nested into the high-resolution atmosphere-ocean coupled general circulation model (MIROC3.2HI AOGCM) for A1B emission scenario. LARS-WG is validated and used to generate 2000 years of daily precipitation from sets of grid-specific parameters derived from the 20-year simulations from the RCMs and statistical downscaling model (SDM: CDFDM). Then 100 samples of the 20-year of continuous precipitation series are resampled, and mean values of precipitation indices are computed, which represents the randomness inherent in daily precipitation data. Based on these samples, the probabilities of change in the indices and the joint occurrence probability of extremes (CDD and Q90) are computed. High probabilities are found for the increases in heavy precipitation amount in spring and summer and elongated consecutive dry days in winter over Japan in the period 2081–2100, relative to 1981–2000. The joint probability increases in most areas throughout the year, suggesting higher potential risk of droughts and excess water-related disasters (e.g., floods) in a 20 year period in the future. The proposed approach offers more flexible way in estimating probabilities of multiple types of precipitation extremes including their joint probability compared to conventional approaches.

Citation: Iizumi, T., I. Takayabu, K. Dairaku, H. Kusaka, M. Nishimori, G. Sakurai, N. N. Ishizaki, S. A. Adachi, and M. A. Semenov (2012), Future change of daily precipitation indices in Japan: A stochastic weather generator-based bootstrap approach to provide probabilistic climate information, *J. Geophys. Res.*, *117*, D11114, doi:10.1029/2011JD017197.

1. Introduction

[2] A serious challenge at providing information to stakeholders regarding possible adaptation to climate change is the uncertainty of climate projection at a regional to local scale. While the Intergovernmental Panel on Climate Change (IPCC) predicts an increase in the frequency of heavy precipitation in East Asia, at a regional scale, a large variation in the sign and amplitude of precipitation change among atmosphere-ocean coupled general circulation models (AOGCMs) are widely reported [*Tebaldi et al.*, 2004;

[1]National Institute for Agro-Environmental Sciences, Tsukuba, Japan.
[2]Meteorological Research Institute, Tsukuba, Japan.
[3]National Research Institute for Earth Science and Disaster Prevention, Tsukuba, Japan.
[4]Graduate School of Life and Environmental Sciences, University of Tsukuba, Tsukuba, Japan.
[5]Center for Computational Science, University of Tsukuba, Tsukuba, Japan.
[6]Research Institute for Global Change, Japan Agency for Marine-Earth Science and Technology, Yokohama, Japan.
[7]Department of Computational and Systems Biology, Rothamsted Research, Harpenden, UK.

Corresponding author: T. Iizumi, National Institute for Agro-Environmental Sciences, 3-1-3 Kannondai, Tsukuba 305-8604, Japan. (iizumit@affrc.go.jp)

Christensen et al., 2007; *Meehl et al.*, 2007]. A similar variation in climate projections can be seen for climate downscaling models, which provide higher spatial and temporal resolution climate data in a limited geographical domain. Changes in regional precipitation and its extremes from dynamical downscaling, i.e., regional climate models (RCMs), and statistical downscaling models (SDMs) vary substantially from one model to another [*Wilby et al.*, 1998; *Frei et al.*, 2006; *Haylock et al.*, 2006; *Schmidli et al.*, 2007].

[3] Probabilistic information on regional precipitation change, such as the United Kingdom Climate Projection (called UKCP09) [*Murphy et al.*, 2009], is useful to support decision making for adaptation in various climate-sensitive sectors under uncertain regional climate projections. However, the limitation of the computer power does not allow generating a full ensemble, which incorporates all possible combinations among GCMs, RCMs, and IPCC emission scenarios [e.g., *Nakicenovic and Swart*, 2000]. Only coordinated research projects such as the Coordinated Regional Climate Downscaling Experiments (CORDEX) and other programs (reviewed in *Arritt and Rummukainen* [2011]) could provide a subset of the full ensemble. Considering these circumstances, efforts have been made to capture the signal of changes in precipitation and its extremes from a limited ensemble of RCMs using perturbed initial conditions [*Huntingford et al.*, 2003; *Kendon et al.*, 2008], boundary conditions from multiple GCMs [*Sato et al.*, 2007], different physical parameterizations setups, multiple RCMs [*Ekström et al.*, 2005; *Takayabu et al.*, 2007], and their combinations [*Frei et al.*, 2006; *Smiatek et al.*, 2009; *Fischer et al.*, 2012]. To this end, many studies fitted a generalized extreme value distribution (GEV) to simulated precipitation extremes for given grid (or area) and applied bootstrap method [*Efron*, 1979] to account for the uncertainty of regional precipitation change associated with the randomness inherent in data [e.g., *Huntingford et al.*, 2003].

[4] Meanwhile, stochastic weather generators (WGs) are tools that can generate daily weather time series at a given site without intensive computation [e.g., *Semenov and Stratonovitch*, 2010]. A conventional use of a WG is (1) to compute parameters of probability distributions of climatic variables from observed daily data at a single site; and (2) generate synthetic daily weather statistically similar to observed. If a WG can accurately represent the statistical characteristics of RCM-simulated daily data, then it can be a powerful tool to provide probabilistic climate information from limited RCM simulations. Among various WGs, LARS-WG was intensively tested over diverse climate zones [*Semenov and Barrow*, 1997; *Qian et al.*, 2005; *Cowden et al.*, 2008; *Allen et al.*, 2010; *Lazzarotto et al.*, 2010; *Luo et al.*, 2010; *Rahman et al.*, 2010; *Semenov et al.*, 2010; *Utset and Del Rio*, 2011] including Asia under monsoon climate [*Bae et al.*, 2008; *Abdulharis et al.*, 2010; *Iizumi et al.*, 2012]. Overall performance of LARS-WG in representing the statistical characteristics of observed precipitation and its extremes at a site was in general good [*Semenov*, 2008; *Qian et al.*, 2008]. Therefore, for this study, we selected LARS-WG as an example.

[5] Projections of regional precipitation changes around Japan substantially vary from one GCM to another, while the multi-GCM ensemble suggests the increased precipitation in summer and transient seasons and decreased precipitation in winter [*Kimoto*, 2005]. If we focus on the projections performed by high-resolution GCMs or RCMs, there is a common tendency for increased mean precipitation averaged over the year and over summer (June–July–August; JJA) in most areas of Japan. In particular, a projection performed by the high-resolution version of the Model for Interdisciplinary Research on Climate (MIROC3.2HI; hereafter referred to as MIROC) AOGCM showed increased precipitation by over 10% around Japan in summer and transient seasons in the end of the 21st century under A1B scenario (2071–2100), relative to 1971–2000 [*Kimoto et al.*, 2005]. An increase in annual (especially, summer) mean precipitation is suggested by the 20 km-mesh global atmospheric model under A1B scenario [*Mizuta et al.*, 2005] and by various combinations of RCMs and GCMs under A2 scenario [*Kurihara et al.*, 2005; *Takayabu et al.*, 2007; *Dairaku et al.*, 2008b].

[6] A somewhat common tendency is seen for increases in the frequency of heavy precipitation in summer, although the geographical distribution of heavy precipitation change varies by GCMs and RCMs, and has a strong dependency on sea surface temperature [*Kusunoki and Mizuta*, 2008]. The projection performed by MIROC AOGCM suggested an increases in the frequency of dry days in winter due to the weakened winter monsoon, and increases in the frequency of heavy precipitation in summer due to the increased activity of the East Asian monsoonal rainband [*Kimoto*, 2005; *Kimoto et al.*, 2005]. A 20-km-mesh global atmospheric model also projected the increases in the annual frequency of heavy precipitation in the western and a part of the northern areas of Japan [*Mizuta et al.*, 2005]. More frequent heavy precipitation over Japan (especially, in the western area) associated with the East Asian monsoonal rainband (called Baiu, it in general occurs during June and July) is suggested by 5-km-mesh RCM [*Yoshizaki et al.*, 2005; *Wakazuki et al.*, 2007]. However, due to large natural climate variability, many studies seem to be suffering from the lack of detection of the robust climate change signal in precipitation extremes from limited high-resolution model simulation.

[7] The main purpose of this study is to propose a new approach to provide probabilistic information on regional precipitation change including extremes that makes use of the LARS-WG to daily precipitation simulated by RCMs and SDMs. Following the main purpose, this study addresses the inter-downscaling model differences in simulated precipitation change over Japan for the end of the 21st century under A1B scenario. Three RCMs (NHRCM, NRAMS, and TWRF; see Table 1 for abbreviations) and a SDM (CDFDM), which are available from the multidownscaling model ensemble formed in the Japanese project of the Multi-Model Ensemble and Downscaling Methods for Assessment of Climate Change Impact (called S-5-3;) [*Arritt and Rummukainen*, 2011; *Ishizaki et al.*, 2012], were considered in this intercomparison. We compared five diagnostics of daily precipitation (referred to as daily precipitation indices) listed in Table 2.

[8] A description of the gridded observed daily precipitation data set, stochastic weather generator, definition of precipitation indices, and proposed approach is included in section 2. Section 3 presents a description of the RCMs and the statistical downscaling model, and climate downscaling experiments setup. Sections 4 and 5 present results of the

Table 1. Acronyms, Types, Institutes, and References for Downscaling Models Used in This Study

Acronym	Type	Model and Institutes	Reference(s)
NHRCM	Dynamical	Operational nonhydrostatic mesoscale model developed by the Japan Meteorological Agency with the Meteorological Research Institute	*Saito et al.* [2006]; *Ishizaki and Takayabu* [2009]
NRAMS	Dynamical	Regional Atmospheric Modeling System version 4.3 modified by the National Research Institute for Earth Science and Disaster Prevention	*Pielke et al.* [1992]; *Dairaku et al.* [2008a, 2008b]; *Emori et al.* [2001]
TWRF	Dynamical	Weather Research and Forecasting model version 3 set up by the Center for Computational Sciences, University of Tsukuba	*Skamarock et al.* [2008]
CDFDM	Statistical	Cumulative distribution function-based downscaling method developed by the National Institute for Agro-Environmental Sciences	*Iizumi et al.* [2010, 2011]

evaluation and simulated precipitation change, respectively. Differences in the simulated precipitation change among downscaling models and the advantages and limitations of the proposed approach are discussed in section 6. Conclusions are presented in section 7.

2. Data Sets and Analysis

2.1. Gridded Observed Daily Precipitation Data Set

[9] Recently, a quality-controlled, high-resolution gridded daily precipitation data set for the Japan area (see Figure 1) (called APHRO_JP) was released [*Kamiguchi et al.*, 2010]. The APHRO_JP data set was obtained by applying a combination of multiple spatial interpolation methods to the gauge data at a densely networked observation sites while considering the effects of orography and network bias on precipitation in mountainous area. For the present-day period (1981–2000), APHRO_JP data set includes gauge data from surface observation sites of the Japan Meteorological Agency (the number of stations varied by year up to a maximum of 158) as well as from over 1300 Automated Meteorological Data Acquisition System (AMeDAS) sites. The quality of daily precipitation data was substantially controlled, based on the system developed in the Japanese project of the Asian Precipitation-Highly Resolved Observational Data Integration Toward Evaluation of Water Resources (APHRODITE) [*Yatagai et al.*, 2008; *Hamada and Yatagai*, 2011]. In this study, daily precipitation data from APHRO_JP was spatially aggregated to the grid interval of 20 km from the original interval of 5 km for consistent comparison with data from the RCMs and SDM. For this study, all daily precipitation values (including zero) at 5-km grid boxes that locate within an intended 20-km grid box were simply averaged. No truncation of a very small daily precipitation value was conducted for the spatially aggregated value.

Table 2. Diagnostics of Daily Precipitation (Daily Precipitation Indices) Used in This Study

Index	Description	Unit
MEA	Mean precipitation	mm/day
FRE	Number of wet days (days with precipitation ≥1 mm/day)	fraction
INT	Mean precipitation amount per wet day	mm/day
CDD	Maximum number of consecutive dry days	days
Q90	90th percentile value of daily precipitation amount in wet days	mm/day

2.2. Daily Precipitation Indices

[10] Five daily precipitation indices that represent daily precipitation characteristics were investigated (Table 2). Namely, (1) mean precipitation, MEA; (2) number of wet days, FRE; (3) mean precipitation amount per wet day, INT, (4) maximum number of consecutive dry days, CDD; and (5) 90th percentile value of daily precipitation amount in wet days, Q90.

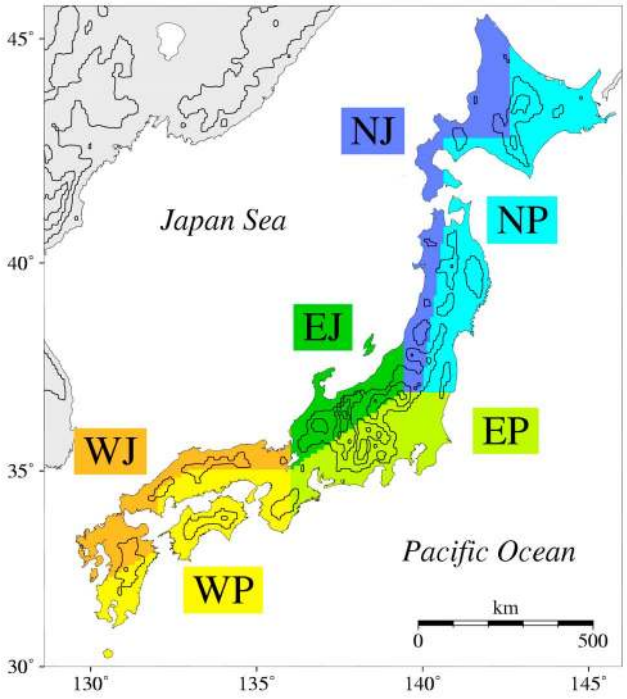

Figure 1. Six areas of Japan where the performance of downscaling models and the simulated change in daily precipitation indices were evaluated. The areas are indicated by the color: Japan Sea side of the Northern, Eastern, and Western Japan (NJ, EJ, and WJ, respectively) and Pacific side of the Northern, Eastern and Western Japan (NP, EP, and WP, respectively). Black line indicates topography at every 500 m.

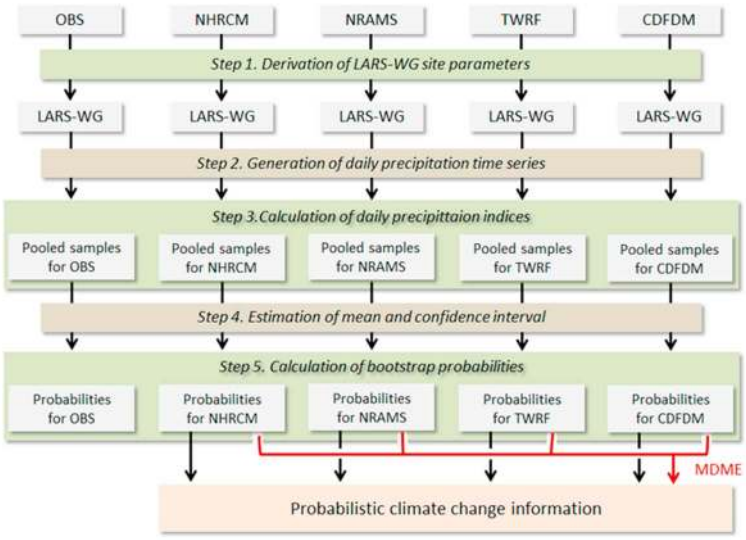

Figure 2. Schematic overview of the WG-based bootstrap approach.

[11] For this study, we defined a day with precipitation ≥1 mm/day as a wet day. All indices except for Q90 were computed month by month and index values for three months were averaged to obtain a seasonal value. The calculated seasonal value was averaged for 20 years, the present-day (1981–2000) and future (2081–2100), and used for analysis. Value of CDD in a particular month was reset to be zero even if a dry series continued from the previous month (thus the maximum value of CDD corresponds to the number of days in a month). Value of Q90 was computed month by month from the empirical cumulative distribution function (CDF) of daily precipitation amount in wet days, consisting of 28–31 days x 20 years. A seasonal mean Q90 value was then calculated by averaging Q90 values for three months. We did not fit any parametric probability distribution, such as a GEV distribution, to avoid any fitting errors. The way of calculation of Q90 could be different from that used in other studies; however, we used it to allow one to consistently compare the results presented here with the results from the perfect boundary condition presented in *Iizumi et al.* [2011]. Thereby, one sample of Q90 was available for each season from 20-year data, whereas 20 samples were available for the indices other than Q90 (i.e., MEA, FRE, INT, and CDD) from the same data.

2.3. LARS-WG

[12] We used a stochastic weather generator LARS-WG version 5 [*Semenov and Stratonovitch*, 2010] for this study. LARS-WG produces daily time series of precipitation, daily maximum and minimum temperatures, solar radiation, and potential evapotranspiration at a specific site. They are based on a set of parameters for probability distributions of climatic variables and correlations between them and were derived from observed daily weather data at given site. In LARS-WG, probability distributions of climatic variables are modeled by using flexible semi-empirical distributions. By modifying parameters for distributions at given site using changes in climatic variables derived from GCMs, RCMs or SDMs, the LARS-WG can generate local-scale daily climate change scenarios that can be used as climate inputs for process-based impact models [e.g., *Iizumi et al.*, 2012]. However, the methodology proposed in this study is different from the conventional use of WGs in climate change studies as described in next section.

2.4. Stochastic Weather Generator-Based Bootstrap Approach

[13] The schematic overview of the proposed approach, the WG-based bootstrap approach, is presented in Figure 2. This approach consists of the following six steps:

[14] *Step* 1: *Derivation of LARS-WG site parameters.* For each 20-km grid box that includes any portion of terrestrial area, a set of site parameters for the distribution of dry/wet series (season by season) and daily precipitation amount in wet days (month by month) were derived from the daily precipitation time series obtained from each downscaling model or observation. If one intends to generate site parameters for daily maximum and minimum temperatures and solar radiation, daily time series for these climatic variables are needed. Also, a set of site parameters were derived from MIROC AOGCM after spatially interpolated to the grid interval of 20 km from the original interval of about 120 km. The site parameters for a given model (the downscaling models or AOGCM) were estimated separately for the present and future climates. For the observation, only the site parameters for the present climate were derived.

[15] *Step* 2: *Generation of daily precipitation time series.* A 2000 year long daily precipitation time series was generated for each grid box, each model or observation, and each climate (the present and future) based on the site parameters. It should be noted that LARS-WG can generate a series of data for as many years as desired (e.g., 2000 years); however, the generated data represent a sample of "typical" years for the period used to estimate site parameters.

[16] *Step* 3: *Calculation of daily precipitation indices.* Values of five daily precipitation indices are calculated as described in section 2.2 from the generated data, resulting in 100 independent samples of mean value for each index, each grid box, each season, each climate, and each model or observation. When calculating an area-mean index value, values at grid boxes that locate within a given area were

spatially averaged. The assumption used here is that, for a single index, values across grid boxes in a given area are perfectly correlated each other, meaning that the maximum (minimum) value of an index in a grid box should appears if a neighboring grid box shows the maximum (minimum) value of the corresponding index. The steps 2–3 correspond to the resampling of mean index values since the proposed approach resamples daily precipitation time series instead of pooled values of an index as did in the previous studies [e.g., *Huntingford et al.*, 2003]. Consequently, the proposed approach can incorporate the randomness inherent in daily precipitation that reflects the natural climate variability observed for the period used to estimate site parameters, whereas the conventional approach using bootstrap method incorporates the natural climate variability by mean of data at a longer (in general yearly) time scale.

[17] *Step* 4: *Estimation of mean and confidence interval.* Mean and a certain confidence interval (90%) are estimated for each index, each grid box (or area), each season, each climate, and each model or observation using the bootstrap method [*Efron*, 1979]. If the observed MEA was taken as the example, 100 samples, $\{MEA_{OBS,1}, MEA_{OBS,2}, \ldots MEA_{OBS,100}\}$, were available. The proposed approach conducts the following procedures:

[18] i. Randomly sample n integer values from {1, 2, …, 100} with replacement. A series of sampled integer values corresponds to $i_1, i_2, \ldots, i_B$ ($B = 10000$);

[19] ii. Then extract values of an intended index of which subscript correspond to sampled integer values, $MEA^{*1}_{OBS} = MEA_{OBS,i_1}$, $MEA^{*2}_{OBS} = MEA_{OBS,i_2}$, …, $MEA^{*B}_{OBS} = MEA_{OBS,i_B}$. These are called bootstrap samples;

[20] iii. Calculate the mean:

$$\overline{MEA}^{*}_{OBS} = \frac{1}{B}\sum_{b=1}^{B} MEA^{*b}_{OBS}; \tag{1}$$

[21] iv. Sort bootstrap samples in ascending order. Let $MEA^{*(p)}_{OBS}$ denotes the pB-th smaller value for the range $0 < p < 1$. If a value of pB is not integer then index values at neighboring two points where values of pB are integer were interpolated.

[22] v. Calculate a certain confidence interval (90%):

$$\left[MEA^{*(0.05)}_{OBS}, MEA^{*(0.95)}_{OBS}\right]; \tag{2}$$

[23] vi. Repeat the procedures i-v for each index, each grid box (or area), each season, each climate, and each model or observation.

[24] *Step* 5: *Estimation of bootstrap probabilities.* Bootstrap samples of an intended index for the future climate are sampled in the similar manner as that in Step 4 i and ii, namely $MEA^{*b}_{NHRCM,future}$ ($b = 1, \ldots, B$), if NHRCM was taken as the example. Then bootstrap probabilities were calculated by counting cases that fall within the following three categories: (1) unprecedentedly positive change, $\Delta MEA^{*b}_{NHRCM,future} > \Delta MEA^{*(0.95)}_{NHRCM,present}$; (2) unprecedentedly negative change, $\Delta MEA^{*b}_{NHRCM,future} < \Delta MEA^{*(0.05)}_{NHRCM,present}$; and (3) within the experienced range, $\Delta MEA^{*(0.05)}_{NHRCM,present} \le \Delta MEA^{*b}_{NHRCM,future} \le \Delta MEA^{*(0.95)}_{NHRCM,present}$. Please note that sampled future changes of a selected model were compared to the confidence interval of the corresponding model to avoid unfavorable impacts of model bias on the probability estimation. For the observation, bootstrap probabilities were calculated only for the present climate. Step 5 is repeated for each index, each grid box (or area), each season, and each model or observation. When one intends to estimate a joint probability of two indices, such as the joint occurrence probability of unprecedentedly positive changes in CDD and Q90, the sampled n integer values (see Step 4 i) were commonly used for bootstrap samples of CDD and Q90 to guarantee that mean values of the two indices were derived from a single 20-year chunk of data. Consequently, the statistical characteristics of the sampled indices (CDD and Q90) were the same with those derived from the original RCM data, indicating that the sampled indices were physically consistent at least 20-year mean level. Bootstrap samples for the four downscaling models (the sample size is 40000) were used to form the multidownscaling model ensemble (MDME). Therefore MDME includes the information on the spread of simulated future change by the downscaling models as well as the randomness inherent in daily precipitation.

3. Models and Experiment

3.1. Regional Climate Models

[25] Three RCMs listed in Table 1 were used for this intercomparison. The RCMs covered the whole of Japan with a common grid interval of 20 km and a nearly common center pole position of the domain, while the domain sizes were slightly different [see *Iizumi et al.*, 2011; *Ishizaki et al.*, 2012]. The initial and lateral boundary conditions, including sea surface temperature and sea ice, were commonly given from MIROC AOGCM outputs under the historical (1981–2000) and A1B scenario experiments (2081–2100). For NHRCM and NRAMS, 3-dimensional data for zonal and meridional winds, air temperature, geopotential height, and specific humidity were used as the boundary conditions. TWRF used relative humidity instead of specific humidity. Additionally, 2-dimensional data for surface pressure, sea level pressure, skin temperature, air temperature and specific humidity (relative humidity for TWRF) at 2 m height, and zonal and meridional winds at 10 m height, soil temperature, soil moisture content, and snow depth were used for the initial surface conditions for the RCMs.

[26] The settings of spin-up and integration differed by the RCMs. Only NRAMS sequentially integrated throughout each 20-year period. Other two performed the downscaling experiments in a manner of time-slice with a 2-month spin-up period as described for the perfect boundary setup [*Iizumi et al.*, 2011]. However, such differences are generally insignificant for long-term downscaling experiments as RCMs depend more on lateral boundary conditions than on initial one [*Castro et al.*, 2005].

[27] For cumulus parameterization, NRAMS and TWRF used the original version of the scheme proposed by *Kain and Fritsch* [1993] (K-F). Only NHRCM used the modified K-F scheme [*Ohmori and Yamada*, 2004; *Narita and Ohmori*, 2007]. For cloud microphysics parameterization, the 3-ice bulk scheme [*Lin et al.* 1983; *Yamada*, 2003], 2-moment scheme [*Walko et al.*, 1995], and single moment 6-class scheme [*Hong et al.*, 2004] was used in NHRCM, NRAMS, and TWRF, respectively. For other parameterizations, such as radiation and planetary boundary layer, the scheme dif-

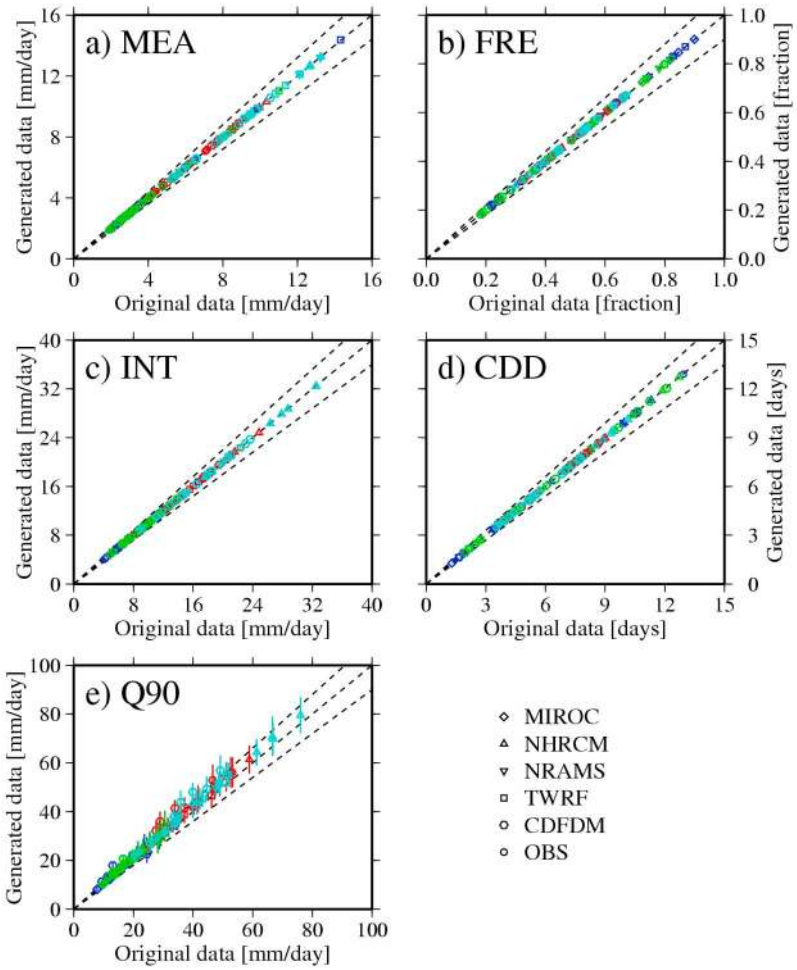

Figure 3. (a–e) Comparisons of 20-year mean value of five daily precipitation indices between the generated and original data from the observation (OBS), GCM (MIROC), RCMs (NHRCM, NRAMS, and TWRF), and SDM (CDFDM) for six areas of Japan. One plot indicates an area of Japan. Vertical line indicates the spread of means among 100 samples (represented by the 90% confidence interval). Dashed lines indicate the 20%-error range. Color indicates the combination of season and climate as below: dark blue, present winter, red, present summer; green, future winter; and right blue, future summer.

fered by the RCMs. More details for RCM setups are available from *Iizumi et al.* [2011] and the references listed in Table 1.

3.2. Statistical Downscaling Method

[28] We used the cumulative distribution function-based downscaling method (CDFDM) [*Iizumi et al.*, 2010, 2011; *Iizumi and Nishimori*, 2011], which falls within the category of "model output statistics (MOS)" that calibrates GCM or RCM daily precipitation against observations [*Maraun et al.*, 2010]. The CDFDM uses daily GCM precipitation as a predictor of local precipitation at a site. The error of MIROC AOGCM in daily precipitation was defined for each percentile of the empirical CDFs provided from the daily GCM and observations (the regridded APHRO_JP data) for the calibration period 1981–2000, grid box by grid box, for each of warm (May–October) and cold (November–April) seasons. The defined GCM error (referred to as the F-e relationship) is then removed from the empirical CDF of the daily GCM outputs for each of the downscaling periods, 1981–2000 and 2081–2100, with the assumption that the F-e relationship does not change with time. This assumption is similar to the stationarity assumption used in other statistical downscaling methods. Compared to quantile-based mapping [*Wood et al.*, 2004], a MOS-type method, it was tested that CDFDM can incorporate changes in maximum precipitation values derived from GCM projections without any additional adjustment [*Iizumi et al.*, 2010; *Iizumi and Nishimori*, 2011]. In contrast, the maximum precipitation values derived from quantile-based mapping are constrained to be equal to those of existing observations, even in future climate conditions unless an additional adjustment is applied for values exceeding the maximum value in the present-day climate.

4. Evaluation of the Simulated Daily Precipitation Indices

4.1. Performance of LARS-WG

[29] To evaluate the performance of LARS-WG in simulating the statistical characteristics of the daily precipitation

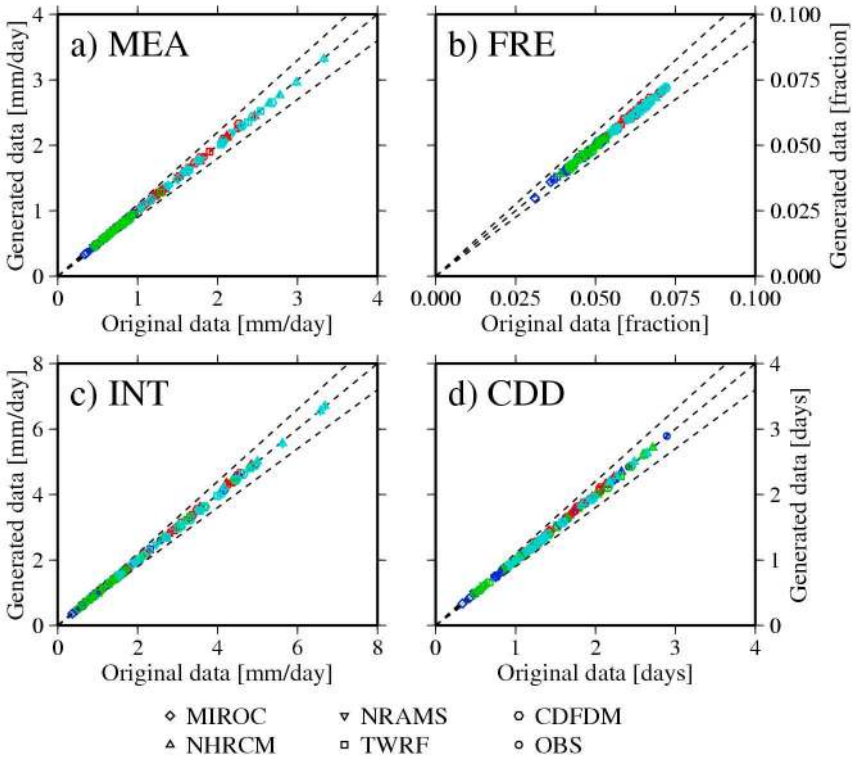

Figure 4. (a–d) Same as Figure 3 but for the standard deviation of seasonal- and area-mean index values during a 20-year period. The standard deviation of Q90 is not available because of the limited sample size of the original data.

indices from the observation, GCM, RCMs, and SDM, we tested (1) whether 20-year means of seasonal- and area-mean indices between two samples (i.e., the generated and original data) can be presume to be the equal using the Student's t-test; and (2) whether the amplitudes of interannual variation (represented by the standard deviation) of seasonal- and area-mean indices for a 20-year period between two samples can be presume to be the equal using the *F* test, as the "overdispersion" problem, a marked tendency to underestimate the interannual variation of seasonal total precipitation, is often addressed for WGs [*Katz and Parlange*, 1998; *Qian et al.*, 2004]. The null hypothesis of the t-test (*F* test) is that the means (variances) of two samples are equal. For each index other than Q90, the two tests were performed 100 times using each of 20-year chunks of data and the original 20-yearlong data (i.e., the sample size for each test was 20). The significance level was set to 5% for both tests. No tests were performed for Q90 because of the limited sample size (only one sample was available for the original data).

[30] The means and standard deviations of the generated and original samples compared are presented in Figures 3 and 4, respectively. A good correspondence in mean between two samples was found for all five indices regardless of the areas, seasons, climates, and models (or observation). Comparatively larger errors compared to the other indices appeared in Q90; however, most generated Q90 values fell within the 20%-error range (Figure 3e). Similar results as the mean were obtained for the comparison in the standard deviations between two samples (Figures 4a–4d), indicating that the "overdispersion" problem is not remarkable for the indices analyzed and its impacts on means are negligible. Furthermore, we validated these results by testing the two null hypotheses mentioned above. In statistical hypothesis testing, the test could falsely reject the null hypothesis with the probability equal to the significance level, even when the null hypothesis is in fact true (known as false positive or type I error [*Semenov et al.*, 2010]). However, while we counted the number of cases that the null hypothesis was rejected, no significant test results was found for both tests regardless of the indices, areas, seasons, climates, and models (or observation). This indicates that LARS-WG accurately captured these statistical characteristics of the indices for the observation, GCM, RCMs, and SDM.

4.2. Seasonal Cycle

[31] The simulated 20-year mean seasonal cycle of the daily precipitation indices, averaged over the terrestrial grid boxes of Japan, is presented in Figure 5. The presented values were computed by averaging over 100 samples of 20-year mean value of the indices from LARS-WG (except 400 samples for MDME). The 90% confidence interval of the indices calculated from the observation using the WG-based bootstrap approach is also shown for reference purposes.

[32] For the mean precipitation (MEA), all models including MDME and parent GCM were distributed within the 90% confidence interval of the observation in most months of the year (Figure 5a), indicating that the models followed the major characteristics of the observed seasonal cycle. However, NRAMS and TWRF simulated far wetter

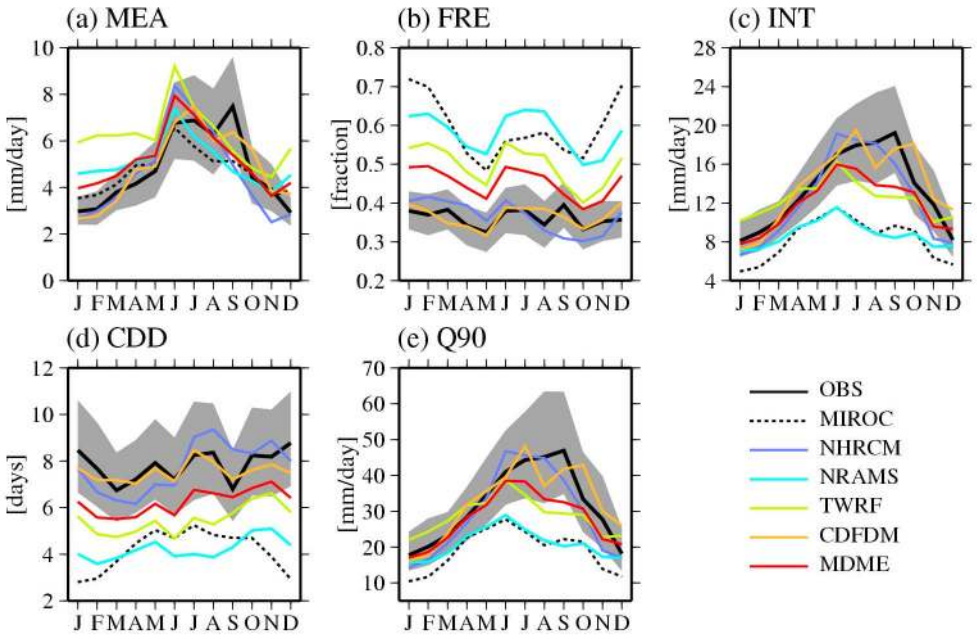

Figure 5. Seasonal cycle of daily precipitation indices for (a) mean precipitation (MEA); (b) number of wet days (FRE); (c) mean precipitation amount per wet day (INT); (d) maximum number of consecutive dry days (CDD); and (e) 90th percentile value of daily precipitation amount in wet days (Q90) for the observation (OBS), parent GCM (MIROC), RCMs (NHRCM, NRAMS, and TWRF), SDM (CDFDM), and multidownscaling model ensemble (MDME). Data were averaged over the terrestrial grids of Japan and 20 years (1981–2000). The gray shaded area indicates the 90% WG-based bootstrap confidence interval of the observation.

conditions in winter (December–January–February; DJF) than the observation. TWRF also largely overestimated mean precipitation in spring (March–April–May; MAM) and early summer (June). All models except for CDFDM failed to capture the one of bimodal wettest conditions in early fall (September) and simulated far drier conditions compared to the observation: this tendency is consistent with that of the parent GCM and MDME. Only NHRCM underestimated mean precipitation throughout the fall (September–October–November; SON). In our case, for MEA, INT, and Q90, the errors associated with the parent GCM seems to be small as the degree of the RCM errors for these indices found are the almost same with those at when the reanalysis data were used for the boundary conditions [*Iizumi et al.*, 2011]. However, the RCM errors for FRE and CDD are comparatively large compared to other indices and the source of the errors could be the parent GCM.

[33] Only NHRCM and CDFDM showed good correspondence in value with the observed FRE in most months of the year (Figure 5b). NRAMS and TWRF and parent GCM simulated more frequent wet days throughout the year. As a result, MDME showed the large overestimation by 21% in annual mean number of wet days.

[34] For the mean precipitation amount per wet day (INT), NHRCM and CDFDM followed the observed seasonal cycle throughout the year (Figure 5c). However, no models captured the single peak of the observation in early fall (September) that might be caused due to autumn rain fronts, typhoons, and their interactions. TWRF overestimated INT by 28% in winter and largely underestimated it by 19% in summer. NRAMS underestimated INT by 34% (on annual mean) throughout the year. Especially, the underestimation is remarkable for NRAMS in summer (43%): this tendency is also seen for the parent GCM.

[35] As expected from the result of FRE, the dry spell (represented by CDD) simulated by NRAMS and TWRF was shorter than that of observation (Figure 5d). A similar tendency was found for the parent GCM. CDFDM showed good correspondence with the observation in terms of value and time variation pattern, while it simulated slightly shorter dry spell in winter. NHRCM failed to capture the time variation pattern of seasonal cycle, but the correspondence in value with the observation is good. MDME underestimated CDD by 19% (on annual mean) throughout the year.

[36] The result of the heavy precipitation amount (represented by Q90) is similar with that of INT. NHRCM, CDFDM, and MDME simulated the major characteristics of the observed seasonal cycle, while these models failed to capture the single peak of Q90 in early fall (September) (Figure 5e). TWRF underestimated Q90 by 21–25% during summer to fall. NRAMS simulated far smaller Q90 (e.g., the underestimation of Q90 approached 42% in summer) throughout the year except for that in winter: this tendency is similar with that of the parent GCM.

4.3. Geographical Pattern

[37] The 20-year mean geographical pattern of the mean winter (DJF) and summer (JJA) CDD derived from the observation, GCM, RCMs, SDM, and MDME is presented in Figure 6. Figure 7 shows the geographical pattern of the

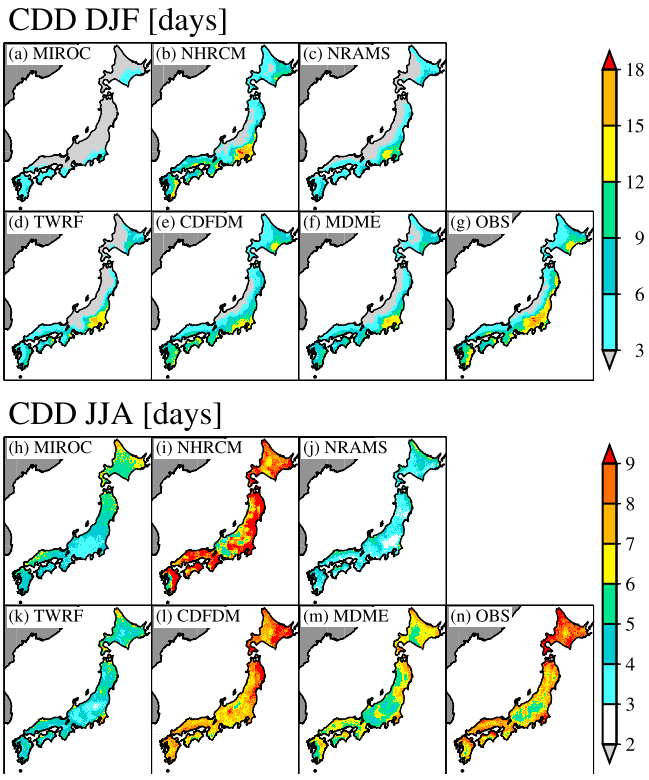

Figure 6. Geographical pattern of mean (a–g) winter (DJF) and (h–n) summer (JJA) maximum number of consecutive dry days (CDD), averaged over the present-day period (1981–2000), for the observation (OBS), parent GCM (MIROC), RCMs (NHRCM, NRAMS, and TWRF), SDM (CDFDM), and multidownscaling model ensemble of the four downscaling models (MDME).

mean winter and summer Q90 in the same manner as Figure 6. Figures for other indices (MEA, FRE, and INT) are omitted to avoid redundancy because the geographical pattern of MEA is similar with that shown in *Iizumi et al.* [2011]. In addition, the geographical pattern of FRE is almost the inverse of that of CDD: this is reasonable because the areas with smaller number of wet days in general have longer dry spell. Additionally, the geographical pattern of INT is almost the same with that of Q90.

[38] For the mean winter dry spell (represented by CDD) (Figures 6a–6g), all downscaling models (NHRCM, NRAMS, TWRF, and CDFDM) and MDME simulated the major characteristics of the observed geographical pattern with clear east–west contrast in dry spell and longest dry spell appear in the inland of the Pacific side of the eastern area (EP; see Figure 1 for abbreviations), while the parent GCM simulated only the east–west gradient of dry spell. In contrast, in summer, while all models including MDME and parent GCM simulated comparatively longer dry spell in the northern areas (NJ and NP) compared to other areas, only NHRCM and CDFDM showed good correspondence in terms of geographical pattern and value (Figures 6h–6n). The correspondence between MDME and the observation is not necessarily good. A consistent result can be seen in Figures 7g and 7h, which presents the seasonal- and area-mean value of the indices for six areas of Japan.

[39] As shown in Figures 7a–7g, all downscaling models captured the major characteristics of the observed mean winter Q90 with heaviest value appear along with the coastal areas in the eastern and western areas (EJ, EP, WJ, and WP). The correspondence of the mean winter Q90 in value between the downscaling models and observation is good in most areas (Figure 8i). In contrast, in summer, the observed heaviest Q90 was distributed in the southwestern slope of the mountains in the eastern and western areas (EJ, EP, WJ, and WP). These characteristics of geographical pattern were accurately simulated by most downscaling models, although NRAMS and TWRF underestimated Q90 in the eastern and western areas (EJ, EP, WJ, and WP; Figure 8j). Almost the same results were seen for INT regardless of winter and summer.

[40] For the mean winter precipitation, the correspondence of the geographical pattern between the downscaling models and observation is good (figure not shown), although NRAMS and TWRF remarkably overestimated the precipitation over Japan, specifically, in the Japan Sea side areas (NJ, EJ, and WJ) (Figure 8a). Meanwhile, all downscaling models more accurately simulated the mean summer precipitation, compared to that of the mean winter precipitation, in terms of the geographical pattern and value (Figure 8b). Overall performance of NHRCM is good, but exceptionally, it overestimated the mean summer precipitation by 36% in the Japan Sea side of the eastern area (EJ).

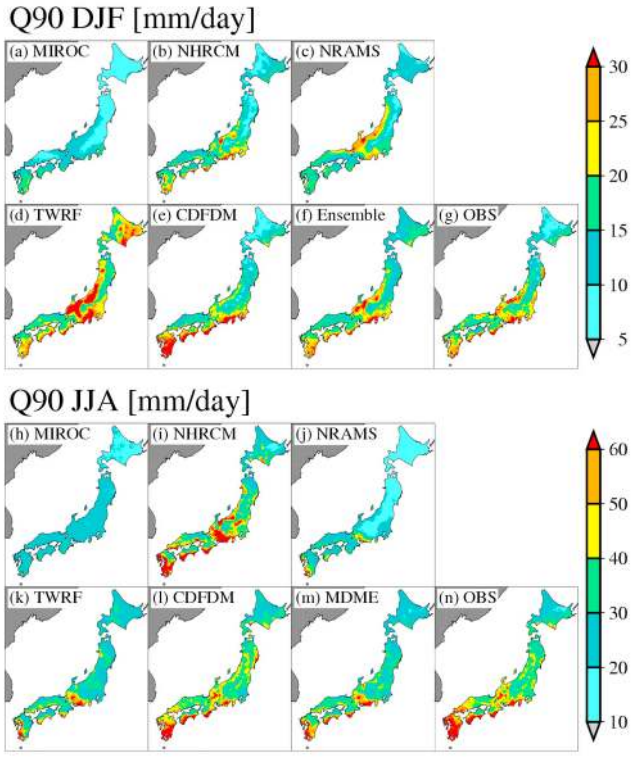

Figure 7. Same as Figure 3 but for the mean (a–g) winter (DJF) and (h–n) summer (JJA) 90th percentile value of daily precipitation amount in wet days (Q90) under the present-day climate condition (1981–2000).

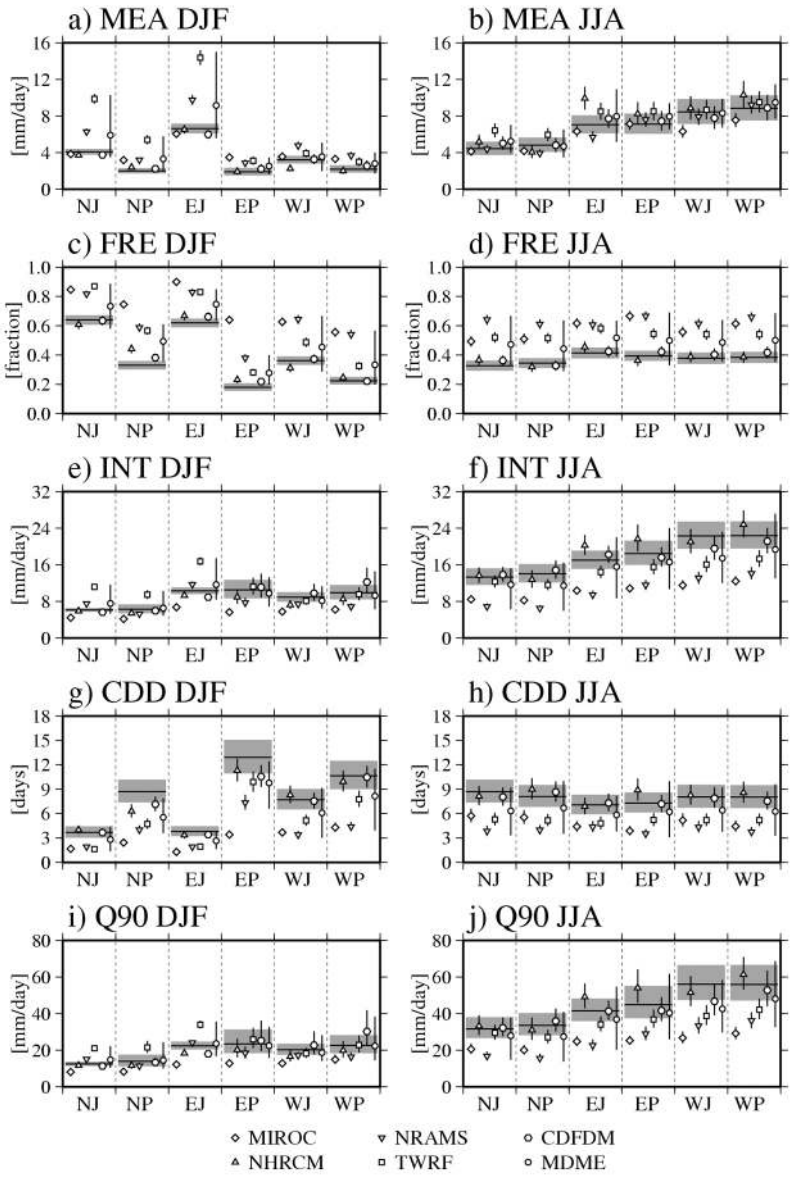

Figure 8. Mean and 90% WG-based bootstrap interval of (a and b) mean winter (DJF) and summer (JJA) precipitation (MEA); (c and d) number of wet days (FRE); (e and f) mean precipitation amount per wet day (INT); (g and h) maximum number of consecutive dry days (CDD); and (i and j) 90th percentile value of daily precipitation amount in wet days (Q90) for the observation (horizontal line and gray shaded area), parent GCM (MIROC; symbol and vertical line), RCMs (NHRCM, NRAMS, and TWRF), SDM (CDFDM), and multidownscaling model ensemble (MDME) for six areas of Japan.

[41] The mean geographical pattern of the observed number of wet days (FRE) has the characteristics that frequent wet days in the Japan Sea side areas (NJ, EJ, and WJ) and less frequent wet days in the Pacific side areas (NP, EP, and WP) in winter and, in summer, frequent wet days in the mountains in the eastern areas (EJ and EP) and the southern slope of the Pacific side of the western area (WP) (figure not shown). For winter, all downscaling models accurately simulated the east–west contrast in FRE. However, the overestimation of FRE by around 30% in the Pacific side areas (NJ, EJ, and WJ) was observed for NRAMS and TWRF (Figure 8c). For summer, NHRCM and CDFDM captured the major characteristics of the observed number of wet days in terms of both geographical pattern and value (Figure 8d). Other downscaling models (NRAMS and TWRF), MDME, and parent GCM overestimated the number of wet days over Japan in summer.

5. Simulated Change in Daily Precipitation Indices

5.1. Seasonal Cycle

[42] Figure 9 presents the simulated change in the 20-year mean seasonal cycle of the daily precipitation indices for the

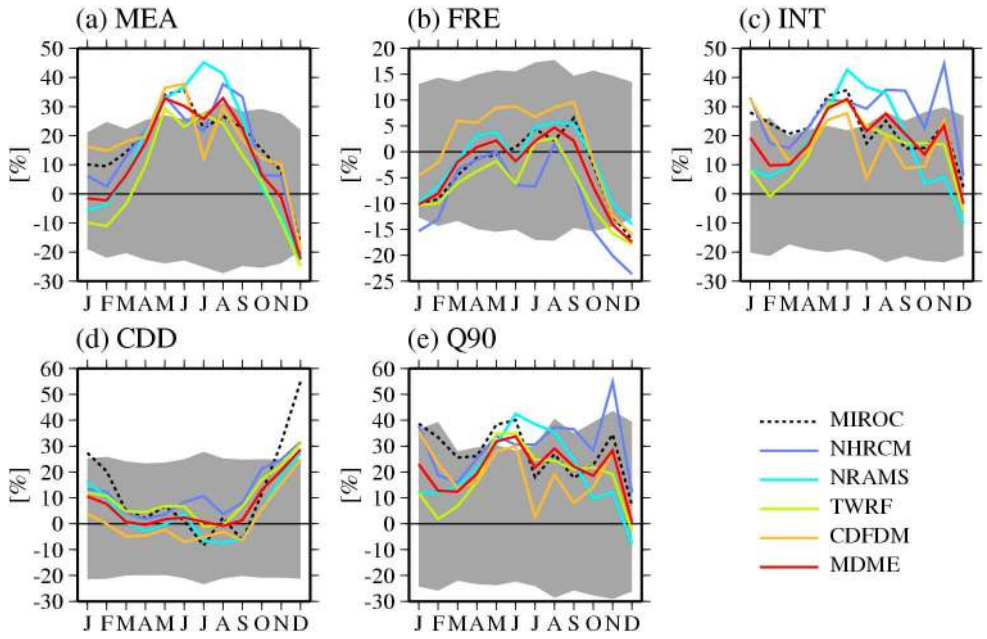

Figure 9. Simulated change (in percent) in the seasonal cycle of (a) mean precipitation (MEA); (b) number of wet days (FRE); (c) mean precipitation amount per wet day (INT); (d) maximum number of consecutive dry days (CDD); and (e) 90th percentile value of daily precipitation amount in wet days (Q90) for the observation (OBS), parent GCM (MIROC), RCMs (NHRCM, NRAMS, and TWRF), statistical downscaling model (CDFDM), and multidownscaling model ensemble (MDME) for the future climate condition (2081–2100, A1B scenario), relative to the period 1981–2000. Data were averaged over the terrestrial grids of Japan and 20 years. The gray shaded area indicates the 90% WG-based bootstrap confidence interval of the observation under the present-day climate condition.

end of the 21st century (2081–2100) under A1B scenario, relative to 1981–2000. The 90% WG-based bootstrap confidence interval, based on the observation, is also shown for reference purposes. In addition, we summarized the probabilities that the simulated future change in the indices falls within the three categories, based on MDME: unprecedentedly negative change, unprecedentedly positive change, and within the present 90% WG-based bootstrap interval (or "within the experienced range").

[43] For the mean precipitation (MEA), all models including MDME and parent GCM simulated the increased precipitation in the middle of spring (April) to the beginning of fall (October) (Figure 9a). Specifically, in the spring and summer, the occurrence probabilities of unprecedentedly wet conditions would greatly increase in all areas to at least 75% (NP, spring) and beyond from the present probability of 5% if we based on MDME (Figure 10 and Table 3). Additionally, all models showed the decreased precipitation in the beginning of winter (December). However, both probabilities of unprecedentedly wet and dry conditions would increase in NJ, NP, and EP, suggesting the increased amplitude of interannual winter precipitation variation during a 20-year period. A similar tendency with that in winter was found for NJ and EJ in fall although the increased probability of unprecedentedly wet conditions appeared in other areas (NP, EP, WJ, and WP) in that season.

[44] All models including MDME and parent GCM showed fewer wet days in winter (Figure 9b). The probability of unprecedentedly few wet days in winter would increase to 74% (NP) to 100% (EJ and WJ) with the decreased probabilities of the other two categories (Figure 10c and Table 3). A somewhat similar tendency with that in winter was found in fall. Meanwhile, in spring and summer, the degree of increase in the probabilities of unprecedentedly few and frequent wet days are moderate compared to those in winter and the highest probability appeared in the category of the "within the experienced range" regardless of the areas (37% for NP in spring to 84% for WJ and WP in spring).

[45] The increased mean precipitation amount per wet day (INT) was simulated throughout the year (exceptions are seen in February and December), especially in the middle of spring (May) to the middle of summer (July) (Figure 9c). Most changes simulated are characterized by the largely increased probability of unprecedentedly intense precipitation in spring, summer, and fall. This tendency is the almost same with that in winter while the increased probability of unprecedentedly weaker precipitation could be seen in NJ, NP, EJ, and WJ in that season.

[46] Almost similar results as INT were found for Q90 (Figure 9e and Table 3). The probabilities of unprecedentedly heavy precipitation (Q90) would increase in all seasons, particularly in summer to 81% (WP) to 98% (EJ).

[47] The simulated change in dry spell (represented by CDD) is small throughout the year except for the middle and end of fall (October and November) and winter. NHRCM simulated the unprecedentedly elongated dry spell through October to December. In addition, TWRF, CDFDM, and

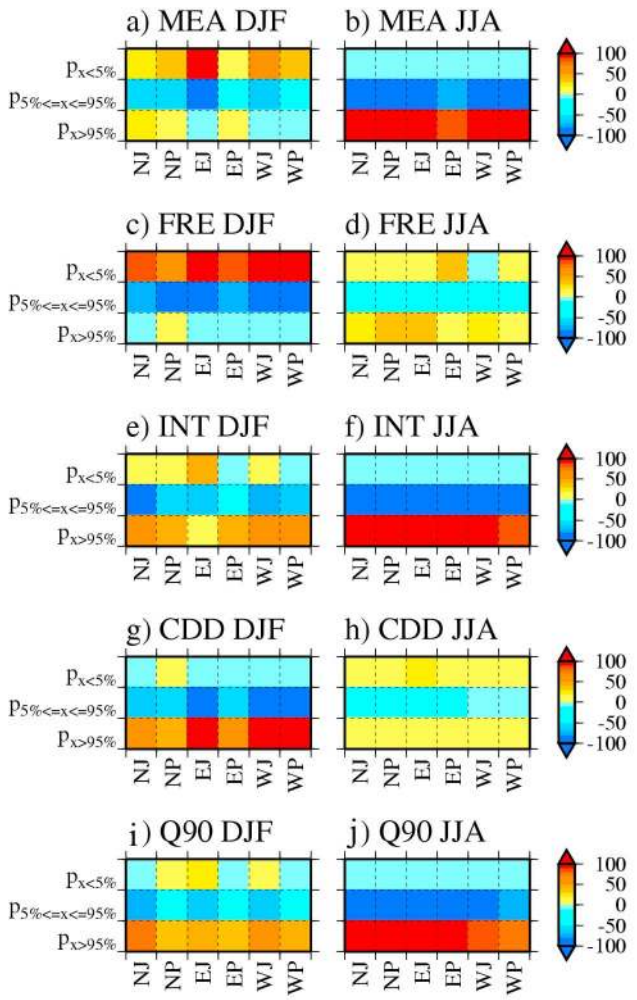

Figure 10. (a–j) Simulated changes in the occurrence probabilities of unprecedentedly positive change ($p_{x>95\%}$), unprecedentedly negative change ($p_{x<5\%}$), and within the experienced range ($p_{5\%\le x\le 95\%}$) in 2081–2100, relative to 1981–2000, for six areas of Japan in winter (DJF) and summer (JJA). The simulated change is presented as the difference in the probability (future minus present). The present probability for each category corresponds to 5% ($p_{x<5\%}$), 90% ($p_{5\%\le x\le 95\%}$), and 5% ($p_{x<95\%}$), respectively.

MDME showed the elongated dry spell in December. As a result of the small change and the discrepancies among the downscaling models, the highest probability appeared in the category of "within the experienced range" in spring and summer, while the probability of unprecedentedly elongated dry spell was simulated to increase to 53% (WP) to 82% (NJ) in fall and to 53% (NP) to 100% (EJ) in winter (Table 3).

[48] The results mentioned above, in particular, increased MEA, INT, and Q90 in summer and transient seasons and decreased in FRE and anticipated elongation in CDD in winter, are consistent with the results obtained from the parent GCM [*Kimoto*, 2005; *Kimoto et al.*, 2005] that are attributed to the strengthening of the subtropical and Okhotsk highs in summer and associated increase in inflow of subtropical moist air around Japan and, in winter, the weakening of northwesterly from Eurasian Continent. The combination of an increased MEA and a slightly decreased FRE in summer leads an increased INT in that season [*Kimoto*, 2005]. These suggest a strong influence of the parent GCM on the downscaled results.

[49] The joint probability of unprecedentedly elongated dry spell (CDD) and unprecedentedly heavy precipitation (Q90) would remain at the same level with the present value in the limited areas (EJ in summer and EP in spring) although it would greatly increase with a large variation by the areas and seasons (Table 4). A great increase in the joint probability emerged in fall (47.1% for EP to 81.7% for NJ) and winter (28.3% for NP to 59.9% for WJ), compared to the present value of around 4.6%. These probabilities are 10 to 17 times larger in fall and 6 to 13 times larger in winter. A comparatively small increase in the joint probability, compared to that in fall and winter, was found in remaining seasons: the joint probability ranges 4.3% (EP) to 26.1% (EJ) in spring and 6.3% (EJ) to 24.0% (EP) in summer. While the degree of the increase in the joint probability in summer is comparatively small, the absolute value of CDD and Q90 in summer is seasonally high as much as that in fall (see Figure 5): this suggests higher potential risk of

Table 3. Probabilities of Change in the Seasonal- and Area-Mean Daily Precipitation Indices for Two Categories[a]

		Winter		Spring		Summer		Fall	
Index	Area	$p_{x<5\%}$	$p_{x>95\%}$	$p_{x<5\%}$	$p_{x>95\%}$	$p_{x<5\%}$	$p_{x>95\%}$	$p_{x<5\%}$	$p_{x>95\%}$
MEA	NJ	31	34	3	**76**	0	**99**	18	31
	NP	**40**	25	1	**75**	0	**99**	1	45
	EJ	**99**	0	0	**87**	0	**100**	**39**	30
	EP	20	7	0	**100**	0	**88**	0	**64**
	WJ	**73**	0	0	**97**	0	**100**	0	**81**
	WP	**36**	1	0	**93**	0	**97**	0	**81**
FRE	NJ	**87**	0	29	9	10	34	**93**	0
	NP	**74**	17	33	30	10	36	**71**	0
	EJ	**100**	0	32	10	6	37	**79**	0
	EP	**86**	0	4	35	40	14	24	20
	WJ	**100**	0	6	11	1	28	43	2
	WP	**100**	0	3	14	8	18	27	17
INT	NJ	24	**65**	0	**97**	0	**100**	1	**78**
	NP	17	**46**	0	**86**	0	**99**	0	**88**
	EJ	**50**	24	0	**100**	0	**99**	15	**66**
	EP	0	46	0	**100**	0	**99**	0	**65**
	WJ	24	**62**	0	**97**	0	**99**	0	**92**
	WP	0	**71**	0	**95**	0	**93**	0	**81**
CDD	NJ	0	**72**	3	26	11	13	0	**82**
	NP	16	**53**	18	18	16	7	0	**61**
	EJ	0	**100**	5	23	28	6	0	**80**
	EP	0	**61**	16	4	8	24	1	47
	WJ	0	**100**	3	8	6	7	0	**64**
	WP	0	**96**	3	9	5	14	1	**53**
Q90	NJ	5	**76**	0	**97**	0	**96**	0	**91**
	NP	14	42	0	**75**	0	**98**	0	**81**
	EJ	28	**51**	0	**100**	0	**98**	3	**67**
	EP	0	38	0	**99**	0	**96**	0	**59**
	WJ	15	**59**	0	**95**	0	**94**	0	**86**
	WP	0	**55**	0	**91**	0	**81**	0	**76**

[a]The categories are unprecedentedly positive change ($p_{x>95\%}$) and unprecedentedly negative change ($p_{x<5\%}$) based on the multidownscaling model ensemble (MDME). The probability (in percent) of the category "within the experienced range" can be calculated by $100 - (p_{x>95\%v} + p_{x<5\%})$. Numbers in bold indicate the category with the highest probability for each index, area, and season. If numbers of both categories are not in bold, the category of "within the experienced range" has the highest probability.

Table 4. Joint Occurrence Probability of Unprecedentedly Positive Seasonal Changes in the Maximum Consecutive Dry Days (CDD) and 90th Percentile Value of Daily Precipitation Amount in Wet Days (Q90) for Six Areas in Japan Under the Present and Changed Climate Conditions[a]

	Present				Future			
Area	DJF	MAM	JJA	SON	DJF	MAM	JJA	SON
NJ	4.8	4.8	4.2	4.7	47.5	26.1	13.1	81.7
NP	4.5	4.6	4.5	4.8	28.3	16.7	7.0	58.4
EJ	4.6	4.2	4.3	4.6	50.6	23.4	6.3	58.7
EP	4.7	4.7	4.5	4.8	37.4	4.3	24.0	47.1
WJ	4.5	4.6	4.6	4.6	59.9	7.8	7.2	64.4
WP	4.3	4.6	4.4	4.6	54.5	8.9	14.3	52.9

[a]Numbers were calculated based on MDME. Present and changed conditions are 1981–2000 and 2081–2100, respectively.

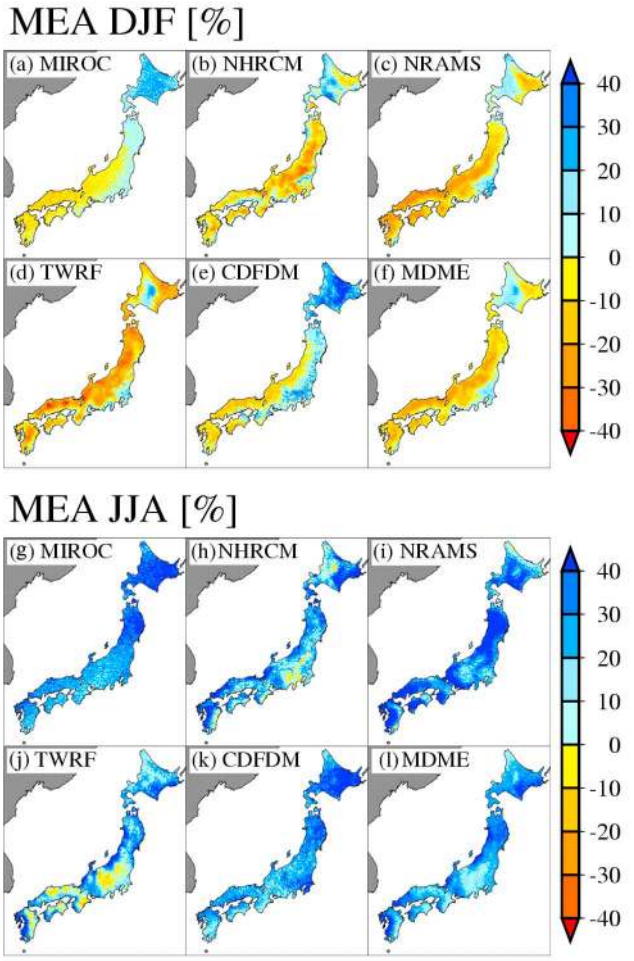

Figure 11. Geographical pattern of the simulated change (in percent) in the mean (a–f) winter (DJF) and (g–l) summer (JJA) mean precipitation (MEA) for the future climate condition (2081–2100, A1B scenario), relative to 1981–2000, for the observation (OBS), parent GCM (MIROC), RCMs (NHRCM, NRAMS, and TWRF), SDM (CDFDM), and multidownscaling model ensemble of the four downscaling models (MDME). Colored area is statistically significant at the 5% confidence level (the Student's t-test with unequal variance assumption was used).

unprecedentedly long CDD events (droughts) and unprecedentedly heavy Q90 events (cause of floods) in a 20year period under the future climate condition.

5.2. Geographical Pattern

[50] The geographical pattern of the simulated change in the mean winter (DJF) and summer (JJA) precipitation (MEA), CDD, and Q90 for the end of the 21st century under A1B scenario (2081–2100), relative to 1981–2000, is presented in Figures 11, 12, and 13, respectively. Figures for other indices (FRE and INT) were omitted to avoid redundancy because the geographical pattern of the simulated change in FRE was just an inverse of that of CDD and the geographical pattern of the simulated change in Q90 was the almost same that of INT. The area-mean simulated change in the mean winter and summer indices is summarized in Figure 14 for six areas of Japan. The 90% WG-based bootstrap confidence interval of the indices calculated from the observation is also shown to compare the amplitude of the simulated mean change in the indices with the error range for the mean associated with the present natural climate variability.

[51] All models including MDME and parent GCM consistently projected the decreased mean winter precipitation

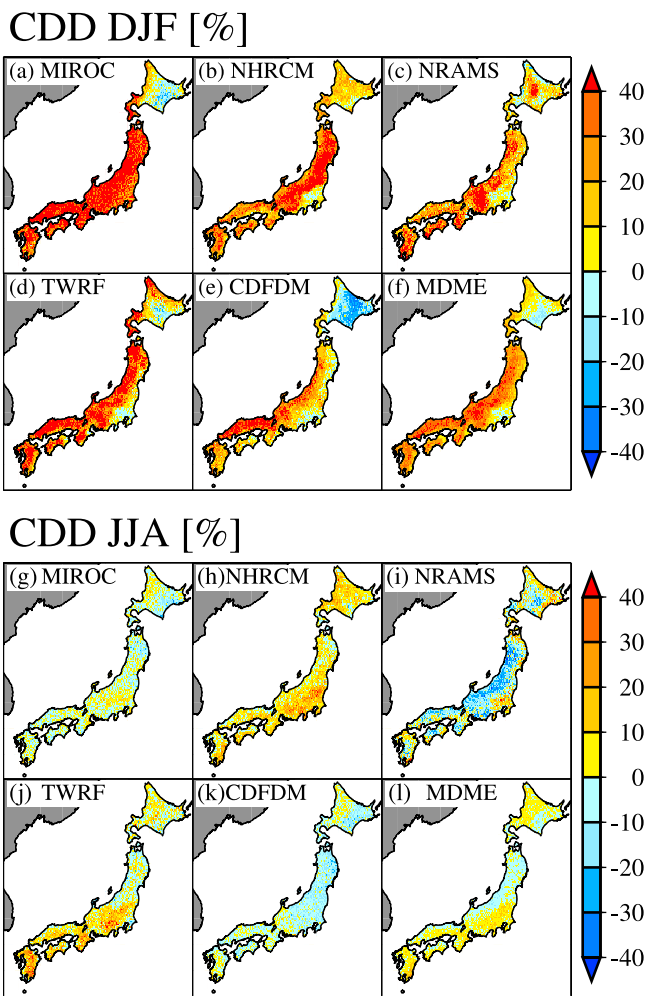

Figure 12. Same as Figure 7 but for the simulated change (in percent) in the mean (a–f) winter (DJF) and (g–l) summer (JJA) maximum number of consecutive dry days (CDD).

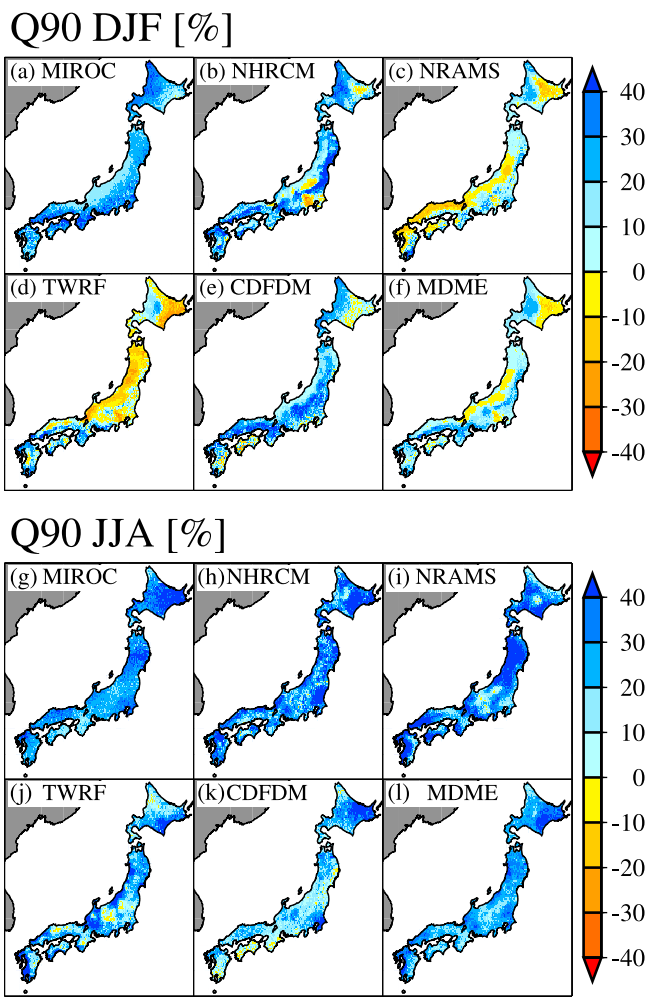

Figure 13. Same as Figure 7 but for the simulated change (in percent) in the mean (a–f) winter (DJF) and (g–l) summer (JJA) 90th percentile value of daily precipitation amount in wet days (Q90).

in the Japan Sea side of the eastern and western areas (EJ and WJ) (Figures 11a–11f). While the SDM (CDFDM) showed the similar geographical pattern of the simulated change in mean winter precipitation with that of the parent GCM, all RCMs (NHRCM, NRAMS, and TWRF) showed different geographical pattern of the simulated change in mean winter precipitation with that of the parent GCM in some areas, such as the Pacific side of the northern area (NP). The parent GCM projection indicates a slight northward shift of the core of winter northwesterly monsoonal flow and this brings an increased mean winter MEA in NP, instead of a decreased mean winter MEA in other areas [*Kimoto*, 2005]. The spread of the downscaled mean winter MEA in NP by the RCMs is therefore in part attributed to the different interactions between the simulated airflow and orography under the strong influence of the northwesterly. In contrast, in summer, all models including MDME and parent GCM consistently simulated the increased mean summer precipitation in most areas of Japan (Figures 11g–11l). As well as the result of the mean winter precipitation, the mean geographical pattern of the simulated change in the mean summer precipitation for CDFDM is similar with that for the parent GCM. In contrast, the RCMs showed different simulated change in the mean summer precipitation with that of the parent GCM in terms of the amplitude of change and geographical pattern.

[52] For dry spell (represented by CDD), all models including MDME and parent GCM consistently simulated the elongated dry spell in winter in most areas of Japan (Figures 12a–12f). However, a large discrepancy of the simulated change in dry spell was observed in the Pacific side of the northern and eastern areas (NP and EP). TWRF, CDFDM, and parent GCM showed the shortened dry spell under the future climate condition in NP in winter, while other models (NHRCM and NRAMS) simulated the elongated dry spell in the area. Furthermore, all downscaling models (NHRCM, NRAMS, TWRF, and CDFDM) showed the shortened dry spell in the leeward side in the Pacific side of the eastern area (EP). In contrast, in summer, the change in dry spell simulated by the parent GCM was small. The simulated change in dry spell varied from one downscaling model to another (Figures 12g–12l). NRAMS and CDFDM simulated the shortened dry spell in many areas, while NHRCM and TWRF simulated the elongated dry spell over many areas. From Figures 14g and 14h, however, both elongated and shortened dry spells in summer under the future climate condition simulated by the downscaling models are smaller than the error range for the mean associated with the present natural climate variability.

[53] The result of the number of wet days (FRE) is almost the inverse of that of CDD. As shown in Figures 14c and 14d, almost all models including MDME and parent GCM simulated the decreased number of wet days in winter in all areas (especially, the Japan Sea side areas (NJ, EJ, and WJ) and the Pacific side of the western Japan (WJ)). In summer, the simulated change in FRE distributed within the range of the present natural climate variability.

[54] The mean geographical pattern of the simulated change in heavy precipitation amount (represented by Q90) varied from one downscaling model to another (Figures 13a–13f). NHRCM and CDFDM showed the increased heavy precipitation amount over Japan in winter (exceptions are seen in NP, WJ, EP, and WP), while NRAMS and TWRF simulated the decreased heavy precipitation amount in many areas of Japan in that season. In contrast, all models including MDME and parent GCM consistently simulated the increased heavy precipitation amount over Japan in summer (Figures 13g–13l). The simulated change in Q90 in summer suggests the unprecedentedly heavy precipitation amount in that season under the future climate condition. The result almost similar with that of Q90 was observed for that of INT regardless of winter and summer.

6. Discussion

6.1. Inter-downscaling Model Differences in Simulated Change

[55] As presented in section 5, there is a large inter-downscaling model differences in the simulated change in the daily precipitation indices in terms of seasonal cycle and geographical pattern. With respect to the simulated change in the seasonal cycle for the future climate condition, the SDM (CDFDM) followed the major characteristics of the

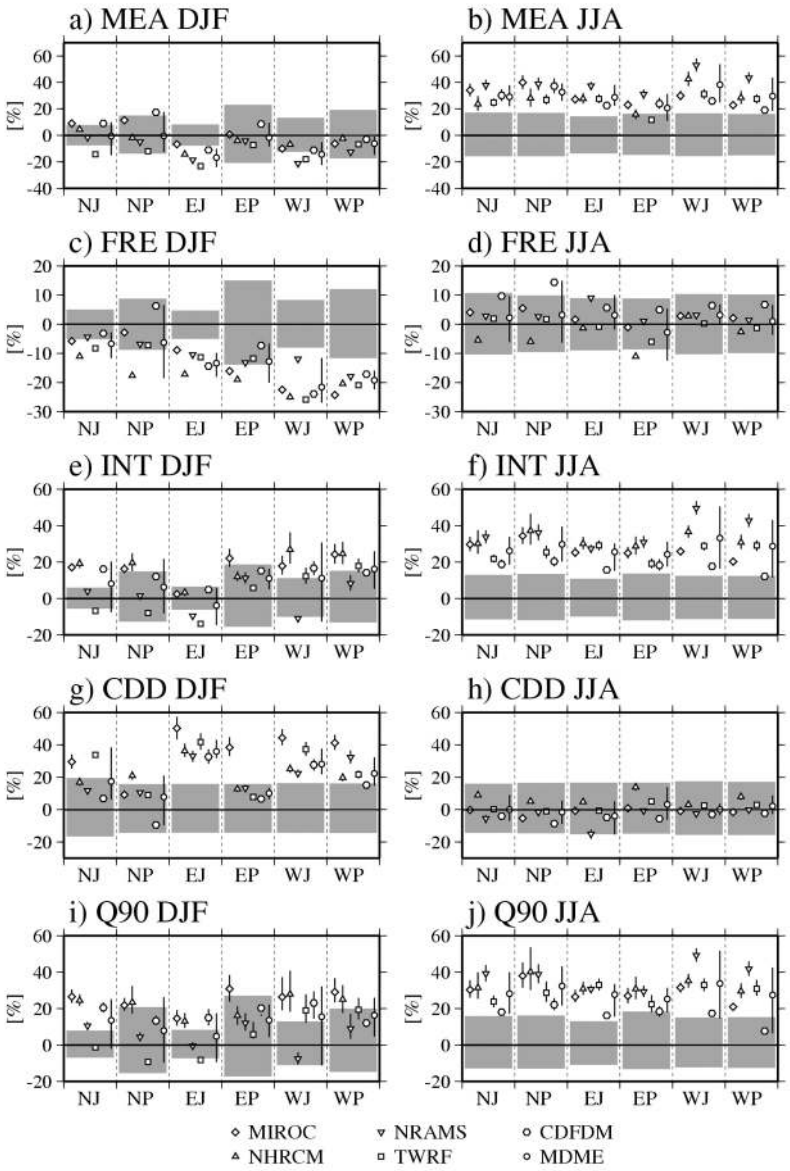

Figure 14. Mean and 90% WG-based bootstrap interval of the simulated change in the (a and b) mean winter (DJF) and summer (JJA) precipitation (MEA); (c and d) number of wet days (FRE); (e and f) mean precipitation amount per wet day (INT); (g and h) maximum number of consecutive dry days (CDD); and (i and j) 90th percentile value of daily precipitation amount in wet days (Q90) for parent GCM (MIROC; symbol and vertical line), RCMs (NHRCM, NRAMS, and TWRF), SDM (CDFDM), and multidownscaling model ensemble (MDME) for six areas of Japan under the future climate condition (2081–2100; A1B scenario), relative to 1981–2000. Gray shaded area indicates the 90% WG-based bootstrap confidence interval of the observation under the present-day climate condition.

change simulated by the parent GCM (Figures 9a–9e). This tendency is consistent among all indices: this is reasonable if we consider the CDFDM algorithm that it has never changed the simulated absolute change in precipitation between the two climate conditions [*Iizumi et al.*, 2010]. Among the RCMs, NRAMS and TWRF tend to follow the change simulated by the parent GCM, compared to that of NHRCM. The change in the indices simulated by NHRCM tends to be slightly different with that of other RCMs. For instance, NHRCM simulated far larger increase in INT and Q90 (Figures 9c and 9e), and the change in CDD simulated by NHRCM is larger than that of other RCMs (Figure 9d).

[56] One possible reason for the differences in the simulated change among the RCMs is the cumulus parameterization; though this is not a definite reason. Only NHRCM used the modified K-F scheme, whereas NRAMS and TWRF used the original version. The better correspondence between NHRCM and observation in FRE and CDD under the present-day climate condition could be attributed to the use of the modified K-F scheme because *Ishizaki et al.* [2012] reported that the modified K-F scheme can reduce

Table 5. Characteristics of the WG-Based Bootstrap Approach in Contrast to a Conventional Approach

	WG-based Bootstrap Approach	Conventional Approach [e.g., *Huntingford et al.*, 2003]
Purpose(s)	It is used to provide the information on the probability of change in multiple quantities of interest (i.e., the daily precipitation indices) including their joint probability with error range associated with the randomness inherent in daily precipitation data (i.e., natural climate variability).	It is used to provide the information on the probability of change in general in single quantity of interest (e.g., annual maxima of multiday precipitation) with error range associated with the randomness inherent in data at in general a yearly time scale.
Assumption(s)	There is no restriction on the type of quantity of interest (e.g., precipitation frequency, intensity, and their combination) and on the shape of probability distribution of quantities of interest.	It is in general applied to a precipitation extreme that is likely follows a GEV.
Pre-processing	It needs to derive LARS-WG site parameters using given models and observation for each of the present and future climates; to generate daily precipitation time series for a certain years (e.g., 2000 years) by using LARS-WG; and to calculate quantities of interest from generated daily precipitation time series.	It needs to calculate a quantity of interest from a given set of daily precipitation data.
Resampling	It resamples daily precipitation time series by using LARS-WG: this corresponds to resampling of multiple quantity of interest with holding the correlation among indices.	It resamples pooled values of a single quantity of interest by using the bootstrap method. Therefore, it is not designed to hold the correlation among multiple quantities of interest unless more sophisticated sampling methods is applied.
Fitting	No fitting is performed to data sampled by using the bootstrap although, in the pre-processing, LARS-WG fits semi-empirical distributions to dry/wet series season by season and to daily precipitation amount in wet days month by month. Semi-empirical distributions are fitted based on daily data for in general 20–30 years.	It fits a GEV to data resampled by using the bootstrap method. One needs to select a probability distribution that is likely suitable for a quantity of interest.

an overestimation of convective rain induced by orography through the refinement of the representation of shallow convection at subgrid scale. This implies that although the RCMs are influenced by the GCM projection, the simulated precipitation characteristics (e.g., FRE) within the calculation domain of some (but not all) RCMs could be improved if the given boundary conditions for humidity and other variables are realistic to some extent.

[57] However, exact reasons why the use of the modified K-F scheme resulted in the decreased number of wet days (and elongated dry spell) under the future climate condition are not clear. In addition, there is a discrepancy in the simulated change in FRE between NRAMS and TWRF, although both RCMs used the original version of K-F scheme. NRAMS showed the increased number of wet days for April to September, while TWRF showed the same tendency only for July to August. These results suggest that the type of cumulus parameterization is not only reason for the differences in the simulated change in FRE and CDD among the RCMs. However, this result is not surprise because the microphysics parameterization, nudging scheme, and other parameterization, such as land surface scheme, radiation scheme, planetary boundary layer scheme, and so on, which could affect the regional precipitation climatology through the land-atmosphere interactions, were all different among the RCMs.

[58] Further study is needed to address exact reasons for the inter-RCM differences in simulated change. Carefully designed climate downscaling experiments are essential to make a progress in this issue. Specifically, climate downscaling experiments using the modified boundary conditions (reanalysis plus spatiotemporally uniform increment of temperature etc.) have potentials to distinguish the source of the inter-RCM differences from various physical parameterization schemes [e.g., *Schär et al.*, 1996].

6.2. Characteristics of the WG-Based Bootstrap Approach

[59] In this study, we demonstrated the unique characteristics of the WG-based bootstrap approach to provide the probabilistic information on regional change in mean precipitation and extremes. A comparison of the proposed approach to approaches used in previous studies [e.g., *Huntingford et al.*, 2003] was made and summarized in Table 5.

[60] First, the advantage of the proposed approach is that WGs can generate a series of daily precipitation data at given grid as many years as desired (e.g., 2000 years) without intensive computation. This corresponds to resampling of daily precipitation time series instead of resampling of seasonal- and area-mean index value (e.g., Q90). Bootstrap is used when additional data is not available, or very expensive to obtain. This is the case for RCMs but not the case for LARS-WG. This feature makes one possible to directly calculate the probability of simulated change in regional mean precipitation as well as extremes from limited RCM or SDM simulation. This makes one free from the signal-to-noise ratio issue, which is always a problem when testing the statistical significance of simulated change in precipitation extremes [e.g., *Kendon et al.*, 2008; *Mizuta et al.*, 2005]. In case of this study, the simulated change in the 20-year mean value of the indices is so large compared to the variance of the mean value estimated from the proposed

approach that the null hypothesis (the difference in the indices between the present and future climates is zero) is rejected. This is reasonable because, from the mathematical point of view, the simulated changes are statistically significant at any confidence level unless LARS-WG site parameters between two climate are the completely same.

[61] Related to the first advantage, the second one is that one can avoid fitting error when estimating the probability distribution of precipitation extremes, such as Q90. As the GEV family has two to three parameters to specify the form and location of distribution, few samples of extremes readily causes fitting error. Additionally, parameter values, especially shape parameter value of GEV, are sensitive to the randomness inherent in data and estimation methods [*Hosking and Wallis*, 1997; *Fujibe*, 2010, 2011]. Direct calculation of Q90 from generated daily precipitation data for many years would be more appropriate to avoid misleading implication from the wrongly fitted GEV distribution: though more quantitative comparison between the proposed approach and GEV fitting approach [e.g., *Huntingford et al.*, 2003] is needed to be conclusive. Additionally, the WG-based bootstrap approach is more flexible because it can simultaneously compute all indices including Q90, while the GEV fitting approach only deals with one quantity of interest (e.g., Q90).

[62] Third, the proposed approach based on the RCM simulation results for the present-day and future climate conditions. This guarantees that the simulated regional precipitation change at a climate time scale (e.g., 20 years) follows the modeled physics (however, we note that the existence of physics is not guaranteed at the time scale shorter than the climate time scale). It is also true for the relationship between multiple indices (e.g., CDD and Q90) at the climate time scale. Additionally, with this setting, there is no need for WGs to assume stationarity. The same holds true for the conventional use of WG. However, the proposed approach puts weight on extracting probabilistic information on climate change signal from limited RCM simulation, while the conventional use of WG puts weight on the generation of local-scale climate change scenarios for impact assessment.

[63] There are some limitations or points where one should be carefully deal with when using the WG-based bootstrap approach. First, this approach heavily relies on the performance of WG. It is known that the performance of WG that uses a parametric distribution, such as a Gamma distribution for daily precipitation amount in wet days, is in general low because such WG has a risk to generate unrealistically large precipitation amount in wet days [*Wallis and Griffiths*, 1995; *Semenov et al.*, 1998]. LARS-WG showed good performance in representing the statistical characteristics of the indices at given grid from the RCMs or SDM, which could in part owe to the flexibility of semi-empirical distribution. In addition, LARS-WG adopts the series approach [*Racsko et al.*, 1991], which uses dry/wet spell in daily precipitation modeling. This also contributes to accurately capture the statistical characteristics of daily precipitation time series in contrast to the modeling based on the two-state Markov chain for precipitation occurrence [e.g., *Sharpley and Williams*, 1990].

[64] Second, many WGs readily available do not consider the spatial correlation among multiple sites (with a few exceptions [e.g., *Wilks*, 2009]). This limits analyses where spatial correlation of precipitation crucial, for instance, predicting total precipitation amount for a given catchment.

[65] Third, we did not account the uncertainty of regional climate change due to decadal and longer climate variability because the transient RCM simulation throughout the 21st century is not readily available. However, as presented in *Iizumi et al.* [2012], it is possible to incorporate such uncertainty into the proposed approach by modifying parameters for distributions of climatic variables year by year on the basis of long-term data.

7. Conclusions

[66] This study proposed and demonstrated a new approach, the WG-based bootstrap approach, to provide the probabilistic regional precipitation change information for Japan from the limited simulations of multidownscaling model ensemble. Additionally, this study intercompares the regional precipitation change scenarios from the ensemble that based on the single GCM and single emission scenario.

[67] The results suggest the following changes in precipitation characteristics (represented by daily precipitation indices) in the period 2081–2100, relative to 1981–2000, based on the climate projection performed by MIROC AOGCM under A1B emission scenario: the greatly increased probabilities of unprecedentedly wet conditions (MEA) and intense precipitation events (INT and Q90) in all areas in spring and summer; the increased probabilities in both unprecedentedly positive and negative changes in FRE and CDD in most areas in spring and summer, i.e., fewer or more frequent wet days (FRE) and shorter or longer dry spell (CDD) in a 20-year period in those seasons; the greatly increased probabilities of unprecedentedly few wet days (FRE) and longer dry spell (CDD) in all areas in fall and winter; and the increased probabilities in both unprecedentedly wet or dry condition (MEA) and more or less intense precipitation events (INT and Q90) during a 20-year period in most areas in winter.

[68] Knowing which aspects of long-term mean daily precipitation, represented by the indices, will exceed the present natural climate variability with their probability could be useful for decision makers when they prioritize potential adaptation measures, although further efforts are essentially needed to account for other major sources of uncertainties for regional climate projection that are not considered in this study (e.g., GCMs, emission scenarios, and other SDMs).

[69] As demonstrated in this study, the WG-based bootstrap approach is a powerful technique to provide the probabilistic information on change in mean precipitation as well as extremes. Long history of the development of WGs makes it possible to accurately capture the statistical characteristics of daily precipitation at given site in various climate zones as well to apply WGs to daily precipitation from RCMs, SDMs, or GCMs. The WG-based bootstrap approach offers a flexible way to detect a climate change signal of regional precipitation extremes from limited RCM, SDM, or high-resolution GCM simulation in a probabilistic manner compared to any other conventional approaches using statistical tests or conventional bootstrap method. While the proposed approach cannot account for all sources

of uncertainties in regional climate projection, this limitation could deal with by applying this approach to ensemble data sets as demonstrated in this study to account for the uncertainty of regional climate change associated with natural climate variability and downscaling model.

[70] **Acknowledgments.** This study was supported by the Global Environmental Research Fund (S-5-3). One author, T. Iizumi, was supported by the Grant-in-Aid Scientific Research (23880030). K. Dairaku and M. Nishimori were in part supported by the Research Program on Climate Change Adaptation (RECCA program). H. Kusaka was in part supported by the Global Environmental Research Fund (S-8). Rothamsted Research receives strategic funding from the Biotechnology and Biological Sciences Research Council of the UK.

References

Abdulharis, A., M. A. Khan, C. Vandana, B. Sandeep, and P. Arvind (2010), Evaluation of LARS-WG for generating long term data for assessment of climate change impact in Bihar, *J. Agrometeorol.*, *12*, 198–201.

Allen, D. M., A. J. Cannon, M. W. Toews, and J. Scibek (2010), Variability in simulated recharge using different GCMs, *Water Resour. Res.*, *46*, W00F03, doi:10.1029/2009WR008932.

Arritt, R. W., and M. Rummukainen (2011), Challenges in regional-scale climate modeling, *Bull. Am. Meteorol. Soc.*, *92*, 365–368, doi:10.1175/2010BAMS2971.1.

Bae, D. H., I. W. Jung, and H. Chang (2008), Potential changes in Korean water resources estimated by high-resolution climate simulation, *Clim. Res.*, *35*, 213–226, doi:10.3354/cr00704.

Castro, C. L., R. A. Pielke, and G. Leoncini (2005), Dynamical downscaling: Assessment of value retained and added using the Regional Atmospheric Modeling System (RAMS), *J. Geophys. Res.*, *110*, D05108, doi:10.1029/2004JD004721.

Christensen, J. H., et al. (2007), Regional climate projections, in *Climate Change 2007: The Physical Science Basis. Contribution of Working Group I to the Fourth Assessment Report of the Intergovernmental Panel on Climate Change*, edited by S. Solomon et al., pp. 847–940, Cambridge Univ. Press, Cambridge, U. K.

Cowden, J. R., D. W. Watkins Jr., and J. R. Mihelcic (2008), Stochastic rainfall modeling in West Africa: Parsimonious approaches for domestic rainwater harvesting assessment, *J. Hydrol.*, *361*, 64–77, doi:10.1016/j.jhydrol.2008.07.025.

Dairaku, K., S. Iizuka, W. Sasaki, A. Beltran, and R. A. Pielke (2008a), Assessment of dynamical downscaling in Japan using an atmosphere-biosphere-river coupling regional climate model, *Eos Trans. AGU*, *89*(53), Fall Meet. Suppl., Abstract GC53A-0687.

Dairaku, K., S. Emori, and T. Nozawa (2008b), Impacts of global warming on hydrological cycles in the Asian monsoon region, *Adv. Atmos. Sci.*, *25*, 960–973, doi:10.1007/s00376-008-0960-1.

Efron, B. (1979), Bootstrap methods: Another look at the jackknife, *Ann. Stat.*, *7*, 1–26, doi:10.1214/aos/1176344552.

Ekström, M., H. J. Fowler, C. G. Kilsby, and P. D. Jones (2005), New estimates of future changes in extreme rainfall across the UK using regional climate model integrations. 2. Future estimates and use in impact studies, *J. Hydrol.*, *300*, 234–251, doi:10.1016/j.jhydrol.2004.06.019.

Emori, S., T. Nozawa, A. Numaguti, and I. Uno (2001), Importance of cumulus parameterization for precipitation simulation over East Asia in June, *J. Meteorol. Soc. Jpn.*, *79*, 939–947, doi:10.2151/jmsj.79.939.

Fischer, A. M., A. P. Weigel, C. M. Buser, R. Knutti, H. R. Künsch, M. A. Liniger, C. Schär, and C. Appenzeller (2012), Climate change projections for Switzerland based on a Bayesian multi-model approach, *Int. J. Climatol.*, doi:10.1002/joc.3396, in press.

Frei, C., R. Schöll, S. Fukutome, J. Schmidli, and P. L. Vidale (2006), Future change of precipitation extremes in Europe: Intercomparison of scenarios from regional climate models, *J. Geophys. Res.*, *111*, D06105, doi:10.1029/2005JD005965.

Fujibe, F. (2010), Assessment of uncertainty in estimating the return periods of extreme rainfalls [in Japanese with English abstract], *Tenki*, *57*, 17–30.

Fujibe, F. (2011), Discussion of fitness analysis for selecting distribution functions in extreme value analysis [in Japanese with English abstract], *Tenki*, *558*, 3–13.

Hamada, A. O. A., and A. Yatagai (2011), An automated quality control method for daily rain-gauge data, *Global Environ. Res*, *15*, 183–192.

Haylock, M. R., G. C. Cawley, C. Harpham, R. L. Wilby, and C. M. Goodess (2006), Downscaling heavy precipitation over the United Kingdom: A comparison of dynamical and statistical methods and their future scenarios, *Int. J. Climatol.*, *26*, 1397–1415, doi:10.1002/joc.1318.

Hong, S.-Y., J. Dudhia, and S.-H. Chen (2004), A revised approach to ice-microphysical processes for the bulk parameterization of cloud and precipitation, *Mon. Weather Rev.*, *132*, 103–120, doi:10.1175/1520-0493(2004)132<0103:ARATIM>2.0.CO;2.

Hosking, J. R. M., and J. R. Wallis (1997), *Regional Frequency Analysis: An Approach Based on L-Moments*, 224 pp., Cambridge Univ. Press, Cambridge, U. K., doi:10.1017/CBO9780511529443.

Huntingford, C., R. G. Jones, C. Prudhomme, R. Lamn, J. H. C. Gash, and D. A. Jones (2003), Regional climate-model predictions of extreme rainfall for a changing climate, *Q. J. R. Meteorol. Soc.*, *129*, 1607–1621, doi:10.1256/qj.02.97.

Iizumi, T., and M. Nishimori (2011), Improvements to statistical climate downscaling simulations by incorporating the APHRO_JP advanced gridded daily precipitation dataset, *Global Environ. Res.*, *15*, 95–102.

Iizumi, T., M. Nishimori, Y. Ishigooka, and M. Yokozawa (2010), Introduction to climate change scenario derived by statistical downscaling [in Japanese with English abstract], *J. Agric. Meteorol.*, *66*, 131–143, doi:10.2480/agrmet.66.2.5.

Iizumi, T., M. Nishimori, K. Dairaku, S. A. Adachi, and M. Yokozawa (2011), Evaluation and intercomparison of downscaled daily precipitation indices over Japan in present-day climate: Strengths and weaknesses of dynamical and bias correction-type statistical downscaling methods, *J. Geophys. Res.*, *116*, D01111, doi:10.1029/2010JD014513.

Iizumi, T., M. A. Semenov, M. Nishimori, Y. Ishigooka, and T. Kuwagata (2012), ELPIS-JP: A dataset of local-scale daily climate change scenarios for Japan, *Philos. Trans. R. Soc. A*, *370*, 1121–1139, doi:10.1098/rsta.2011.0305.

Ishizaki, N., and I. Takayabu (2009), On the warming events over Toyama plain by using NHRCM, *Sci. Online Lett. Atmos.*, *5*, 129–132, doi:10.2151/sola.2009-033.

Ishizaki, N., et al. (2012), Inter-comparison of the skill in the Japan region of five RCMs nested in JRA-25, *J. Meteorol. Soc. Jpn.*, in press.

Kain, J. S., and J. M. Fritsch (1993), Convective parameterization for mesoscale models: The Kain-Fritsch scheme, in *The Representation of Cumulus Convection in Numerical Models*, *Meteorol Monogr. Ser.*, vol. 24, edited by K. Emanuel and D. J. Raymond, pp. 165–170, Am. Meteorol. Soc., Washington, D. C.

Kamiguchi, K., O. Arakawa, A. Kitoh, A. Yatagai, A. Hamada, and N. Yasutomi (2010), Development of APHRO_JP, the first Japanese high-resolution daily precipitation product for more than 100 years, *Hydrol. Res. Lett.*, *4*, 60–64, doi:10.3178/hrl.4.60.

Katz, R. W., and M. B. Parlange (1998), Overdispersion phenomenon in stochastic modeling of precipitation, *J. Clim.*, *11*, 591–601, doi:10.1175/1520-0442(1998)011<0591:OPISMO>2.0.CO;2.

Kendon, E. J., D. P. Rowell, R. G. Jones, and E. Buonomo (2008), Robustness of future changes in local precipitation extremes, *J. Clim.*, *21*, 4280–4297, doi:10.1175/2008JCLI2082.1.

Kimoto, M. (2005), Simulated change of the East Asian circulation under global warming scenario, *Geophys. Res. Lett.*, *32*, L16701, doi:10.1029/2005GL023383.

Kimoto, M., N. Yasutomi, C. Yokoyama, and S. Emori (2005), Projected changes in precipitation characteristics around Japan under the global warming, *Sci. Online Lett. Atmos.*, *1*, 85–88, doi:10.2151/sola.2005-023.

Kurihara, K., K. Ishihara, H. Sasaki, Y. Fukuyama, H. Saitou, I. Takayabu, K. Murazaki, Y. Sato, S. Yukimoto and A. Noda (2005), Projection of climatic change over Japan due to global warming by high-resolution regional climate model in MRI, *Sci. Online Lett. Atmos.*, *1*, 97–100, doi:10.2151/sola.2005.026.

Kusunoki, K., and R. Mizuta (2008), Future changes in the Baiu rain band projected by a 20-km mesh global atmospheric model: Sea surface temperature dependence, *Sci. Online Lett. Atmos.*, *4*, 85–88.

Lazzarotto, P., P. Calanca, M. A. Semenov, and J. Fuhrer (2010), Transient responses to increasing CO_2 and climate change in an unfertilized grass-clover sward, *Clim. Res.*, *41*, 221–232, doi:10.3354/cr00847.

Lin, Y.-L., R. D. Farley, and H. D. Orville (1983), Bulk parameterization of the snow fields in a cloud model, *J. Clim. Appl. Meteorol.*, *22*, 1065–1092, doi:10.1175/1520-0450(1983)022<1065:BPOTSF>2.0.CO;2.

Luo, Q., W. Bellotti, P. Hayman, M. Williams, and P. Devoil (2010), Effects of changes in climatic variability on agricultural production, *Clim. Res.*, *42*, 111–117, doi:10.3354/cr00868.

Maraun, D., et al. (2010), Precipitation downscaling under climate change: Recent developments to bridge the gap between dynamical models and the end user, *Rev. Geophys.*, *48*, RG3003, doi:10.1029/2009RG000314.

Meehl, G. A., et al. (2007), Global climate projections, in *Climate Change 2007: The Physical Science Basis. Contribution of Working Group I to the Fourth Assessment Report of the Intergovernmental Panel on Climate Change*, edited by S. Solomon et al., pp. 747–845, Cambridge Univ. Press, Cambridge, U. K.

Mizuta, R., T. Uchiyama, K. Kamiguchi, A. Kitoh, and A. Noda (2005), Changes in extremes indices over Japan due to global warming projected

by a global 20-km-mesh atmospheric model, *Sci. Online Lett. Atmos.*, *1*, 153–156, doi:10.2151/sola.2005-040.

Murphy, J. M., et al. (2009), UK climate projections science report: Climate change projections, Hadley Cent., Met Off., Exeter, U. K.

Nakicenovic, N., and R. Swart (2000), *Special Report on Emissions Scenarios: A Special Report of Working Group III of the Intergovernmental Panel on Climate Change*, Cambridge Univ. Press, Cambridge, U. K.

Narita, M., and S. Ohmori (2007), Improving precipitation forecasts by the operational nonhydrostatic mesoscale model with the Kain-Fritsch convective parameterization and cloud microphysics, paper presented at 12th Conference on Mesoscale Processes, Am. Meteorol. Soc., Waterville Valley, N. H.

Ohmori, S., and Y. Yamada (2004), Implementation of the Kain-Fritsch convective parameterization scheme in the JMA's non-hydrostatic model, World Meteorol. Organ., Geneva, Switzerland.

Pielke, R. A., et al. (1992), A comprehensive meteorological modeling system: RAMS, *Meteorol. Atmos. Phys.*, *49*, 69–91, doi:10.1007/BF01025401.

Qian, B., S. Gameda, H. Hayhoe, R. De Jong, and A. Bootsma (2004), Comparison of LARS-WG and AAFC-WG stochastic weather generators for diverse Canadian climates, *Clim. Res.*, *26*, 175–191, doi:10.3354/cr026175.

Qian, B., H. Hayhoe, and S. Gameda (2005), Evaluation of the stochastic weather generators LARS-WG and AAFC-WG for climate change impact studies, *Clim. Res.*, *29*, 3–21, doi:10.3354/cr029003.

Qian, B., S. Gameda, and H. Hayhoe (2008), Performance of stochastic weather generators LARS-WG and AAFC-WG for reproducing daily extremes of diverse Canadian climates, *Clim. Res.*, *37*, 17–33, doi:10.3354/cr00755.

Racsko, P., L. Szeidl, and M. A. Semenov (1991), A serial approach to local stochastic weather models, *Ecol. Modell.*, *57*, 27–41, doi:10.1016/0304-3800(91)90053-4.

Rahman, M., T. Bolisetti, and R. Balachandar (2010), Effect of climate change on low-flow conditions in the Ruscom River watershed, Ontario, *Trans. ASABE*, *53*, 1521–1532.

Saito, K., et al. (2006), The operational JMA nonhydrostatic mesoscale model, *Mon. Weather Rev.*, *134*, 1266–1298, doi:10.1175/MWR3120.1.

Sato, T., F. Kimura, and A. Kitoh (2007), Projection of global warming onto regional precipitation over Mongolia using a regional climate model, *J. Hydrol.*, *333*, 144–154, doi:10.1016/j.jhydrol.2006.07.023.

Schär, C., C. Frei, D. Lüthi, and H. C. Davies (1996), Surrogate climate-change scenarios for regional climate models, *Geophys. Res. Lett.*, *23*(6), 669–672, doi:10.1029/96GL00265.

Schmidli, J., C. M. Goodess, C. Frei, M. R. Haylock, Y. Hundecha, J. Ribalaygua, and T. Schmith (2007), Statistical and dynamical downscaling of precipitation: An evaluation and comparison of scenarios for the European Alps, *J. Geophys. Res.*, *112*, D04105, doi:10.1029/2005JD007026.

Semenov, M. A. (2008), Simulation of weather extreme events by stochastic weather generator, *Clim. Res.*, *35*, 203–212, doi:10.3354/cr00731.

Semenov, M. A., and E. M. Barrow (1997), Use of a stochastic weather generator in the development of climate change scenarios, *Clim. Change*, *35*, 397–414, doi:10.1023/A:1005342632279.

Semenov, M. A., and P. Stratonovitch (2010), Use of multi-model ensembles from global climate models for impact assessments of climate change, *Clim. Res.*, *41*, 1–14, doi:10.3354/cr00836.

Semenov, M. A., R. J. Brooks, E. M. Barrow, and C. W. Richardson (1998), Comparison of the WGEN and LARS-WG stochastic weather generators for diverse climates, *Clim. Res.*, *10*, 95–107, doi:10.3354/cr010095.

Semenov, M. A., M. Donatelli, P. Stratonovitch, E. Chatzidaki, and B. Baruth (2010), ELPIS: A dataset of local-scale daily climate scenarios for Europe, *Clim. Res.*, *44*, 3–15, doi:10.3354/cr00865.

Sharpley, A. N., and J. R. Williams (1990), EPIC-erosion/productivity impact calculator. 1. Model documentation, *Tech. Bull. 1768*, U. S. Dep. of Agric., Washington, D. C.

Skamarock, W. C., J. B. Klemp, J. Dudhia, D. O. Gill, D. M. Barker, M. G. Duda, X.-Y. Huang, W. Wang, and J. G. Powers (2008), A description of the Advanced Research WRF version 3, *Tech. Note TN-475*, Natl. Cent. for Atmos. Res., Boulder, Colo.

Smiatek, G., H. Kunstmann, R. Knoche, and A. Marx (2009), Precipitation and temperature statistics in high-resolution regional climate models: Evaluation for the European Alps, *J. Geophys. Res.*, *114*, D19107, doi:10.1029/2008JD011353.

Takayabu, I., H. Kato, K. Nishizawa, Y. N. Takayabu, Y. Sato, H. Sasaki, K. Kurihara, and A. Kitoh (2007), Future projections in precipitation over Asia simulated by two RCMs nested into MRI-CGCM2.2, *J. Meteorol. Soc. Jpn.*, *85*, 511–519, doi:10.2151/jmsj.85.511.

Tebaldi, C., L. O. Mearns, D. Nychka, and R. L. Smith (2004), Regional probabilities of precipitation change: A Bayesian analysis of multimodel simulations, *Geophys. Res. Lett.*, *31*, L24213, doi:10.1029/2004GL021276.

Utset, A., and B. Del Rio (2011), Reliability of current Spanish irrigation designs in a changed climate: A case study, *J. Agric. Sci.*, *149*, 171–183, doi:10.1017/S0021859610001073.

Wakazuki, Y., S. Kanada, C. Muroi, A. Hashimoto, T. Kato, M. Nakamura, A. Noda, M. Yoshizaki, and K. Yasunaga (2007), Regional climate projection experiments on the Baiu frontal activity around the Japan Islands using a non-hydrostatic cloud-system-resolving model, *J. Earth Simulator*, *8*, 13–25.

Walko, R. L., W. R. Cotton, M. P. Meyers, and J. Y. Harrington (1995), New RAMS cloud microphysics parameterization. Part II: The two-moment scheme, *Atmos. Res.*, *38*, 29–62, doi:10.1016/0169-8095(94)00087-T.

Wallis, T. W. R., and J. F. Griffiths (1995), An assessment of the weather generator (WXGEN) used in the erosion/productivity impact calculator (EPIC), *Agric. For. Meteorol.*, *73*, 115–133, doi:10.1016/0168-1923(94)02172-G.

Wilby, R. L., T. M. L. Wigley, D. Conway, P. D. Jones, B. C. Hewitson, J. Main, and D. S. Wilks (1998), Statistical downscaling of general circulation model output: A comparison of methods, *Water Resour. Res.*, *34*, 2995–3008, doi:10.1029/98WR02577.

Wilks, D. S. (2009), A gridded multisite weather generator and synchronization to observed weather data, *Water Resour. Res.*, *45*, W10419, doi:10.1029/2009WR007902.

Wood, A. W., L. R. Leung, V. Sridhar, and D. P. Lettenmaier (2004), Hydrological implications 769 of dynamical and statistical approaches to downscaling climate model outputs, *Clim. Change*, *62*, 189–216, doi:10.1023/B:CLIM.0000013685.99609.9e.

Yamada, Y. (2003), Cloud microphysics. The JMA nonhydrostatic model [in Japanese], *Jpn. Meteorol. Agency Annu. Rep.*, *49*, 52–76.

Yatagai, A., P. Alpert, and P. Xie (2008), Development of a daily gridded precipitation data set for the Middle East, *Adv. Geosci.*, *12*, 165–170, doi:10.5194/adgeo-12-165-2008.

Yoshizaki, M., C. Muroi, S. Kanada, Y. Wakazuki, K. Yasunaga, A. Hashimoto, T. Kato, K. Kurihara, A. Noda, and S. Kusunoki (2005), Changes in Baiu (Mei-yu) frontal activity in the global warming climate simulated by a non-hydrostatic regional model, *Sci. Online Lett. Atmos.*, *1*, 25–28, doi:10.2151/sola.2005-008.